Cell Reports

Article

A nociceptive neuronal ensemble in the dorsomedial prefrontal cortex underlies pain chronicity

Graphical abstract

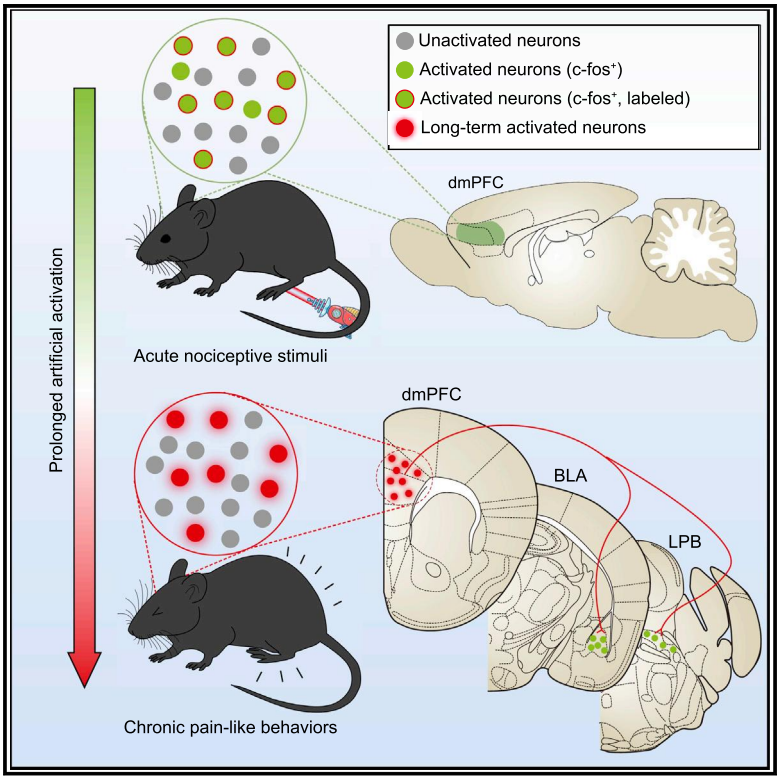

Authors

Xuetao Qi, Kun Cui, Yu Zhang, ...,
Jie Zheng, Ming Yi, You Wan

Correspondence

mingyi@hsc.pku.edu.cn (M.Y.),
ywan@hsc.pku.edu.cn (Y.W.)

In brief

Qi et al. demonstrate that a nociceptive neuronal ensemble in the dorsomedial prefrontal cortex is crucial for pain chronicity, and identify basolateral amygdala and lateral parabrachial nuclei as major downstream targets of this ensemble.

Highlights

- Acute nociceptive stimuli activate a neuronal ensemble in dmPFC
- dmPFC nociceptive ensemble shows elevated activity to noxious stimuli in chronic pain
- Prolonged activation of dmPFC nociceptive ensemble induces chronic pain-like behavior
- dmPFC nociceptive ensemble modulates pain-related downstream regions

Qi et al., 2022, Cell Reports *41*, 111833
December 13, 2022
https://doi.org/10.1016/j.celrep.2022.111833

CellPress

Cell Reports

CellPress
OPEN ACCESS

Article

A nociceptive neuronal ensemble in the dorsomedial prefrontal cortex underlies pain chronicity

Xuetao Qi,[1] Kun Cui,[1] Yu Zhang,[2] Linshu Wang,[1] Jifu Tong,[1] Weiqi Sun,[1] Shan Shao,[1] Jiaxin Wang,[1] Cheng Wang,[3] Xiaoyan Sun,[1] Liming Xiao,[4] Ke Xi,[1] Shuang Cui,[1,5] Fengyu Liu,[1,5] Longyu Ma,[1,5] Jie Zheng,[1,5] Ming Yi,[1,5,7,*] and You Wan[1,5,6,*]

[1]Neuroscience Research Institute and Department of Neurobiology, School of Basic Medical Sciences, Peking University, Beijing 100083, P.R. China

[2]NHC Key Laboratory of Human Disease Comparative Medicine, Institute of Laboratory Animal Sciences, CAMS&PUMC, Beijing 100021, P.R. China

[3]Chinese Institute for Brain Research, Beijing (CIBR), Beijing 102206, P.R. China

[4]Institute of Systems Biomedicine, Department of Medical Bioinformatics, School of Basic Medical Sciences, Peking University Health Science Center, Beijing 100083, P.R. China

[5]Key Laboratory for Neuroscience, Ministry of Education/National Health Commission, Peking University, Beijing 100083, P.R. China

[6]Co-innovation Center of Neuroregeneration, Nantong University, Nantong 226001, P.R. China

[7]Lead contact

*Correspondence: mingyi@hsc.pku.edu.cn (M.Y.), ywan@hsc.pku.edu.cn (Y.W.)

https://doi.org/10.1016/j.celrep.2022.111833

SUMMARY

Pain chronicity involves unpleasant experience in both somatosensory and affective aspects, accompanied with the prefrontal cortex (PFC) neuroplastic alterations. However, whether specific PFC neuronal ensembles underlie pain chronicity remains elusive. Here we identify a nociceptive neuronal ensemble in the dorsomedial prefrontal cortex (dmPFC), which shows prominent reactivity to nociceptive stimuli. We observed that this ensemble shows distinct molecular characteristics and is densely connected to pain-related regions including basolateral amygdala (BLA) and lateral parabrachial nuclei (LPB). Prolonged chemogenetic activation of this nociceptive neuronal ensemble, but not a randomly transfected subset of dmPFC neurons, induces chronic pain-like behaviors in normal mice. By contrast, silencing the nociceptive dmPFC neurons relieves both pain hypersensitivity and anxiety in mice with chronic inflammatory pain. These results suggest the presence of specific dmPFC neuronal ensembles in processing nociceptive information and regulating pain chronicity.

INTRODUCTION

While acute pain evokes protective behavioral responses to actual or potential tissue injury, chronic pain causes perceptual, affective, and cognitive problems and excruciates about 20% of the human population worldwide.[1,2] However, the neurobiological mechanisms underlying pain chronicity, the transfer from acute to chronic pain, remain poorly defined. Multiple levels of neural malfunction in pain chronicity have been unraveled from peripheral afferents, to spinal cord and brain.[3,4]

Given that pain is gradually overgeneralized from sensory to emotional and cognitive dimensions,[5] the limbic system is believed to be involved in both processing nociceptive information under physiological conditions and regulating pain chronicity with dramatic neuroplastic changes.[3,6] Specifically, the dorsomedial prefrontal cortex (dmPFC) plays a crucial role during pain chronicity. Human imaging studies have shown specific correlativity between dmPFC activity and pain intensity in patients with chronic back pain[7] and pain rumination in idiopathic temporomandibular disorder.[8] Altered morphology and increased excitability of dmPFC are also observed in rodents during chronic pain.[9,10]

However, substantial controversies exist on the mechanisms of how dmPFC regulates pain chronicity. In rodents, the dmPFC includes the prelimbic cortex (PrL) and the rostral anterior cingulate cortex (rACC) subregions. While the rACC is hyperactive and exhibits prominent regulatory ability on chronic pain-associated hypersensitivity and negative emotions,[11–16] conflicting results are reported regarding the PrL. Bilateral lesions of PrL in rats relieve heat hyperalgesia,[17] while activation of PrL aggravates nociceptive responses in rats with chronic inflammatory pain experience.[18] However, suppressed excitability of PrL layer 5 neurons and decreased PrL-periaqueductal gray (PAG) connectivity in chronic pain are reported in other studies.[19–22] Hence, how PrL neurons alter in and contribute to chronic pain significantly varies across studies, as both enhanced and suppressed excitability/activity changes have been reported.[9,10,17,23,24]

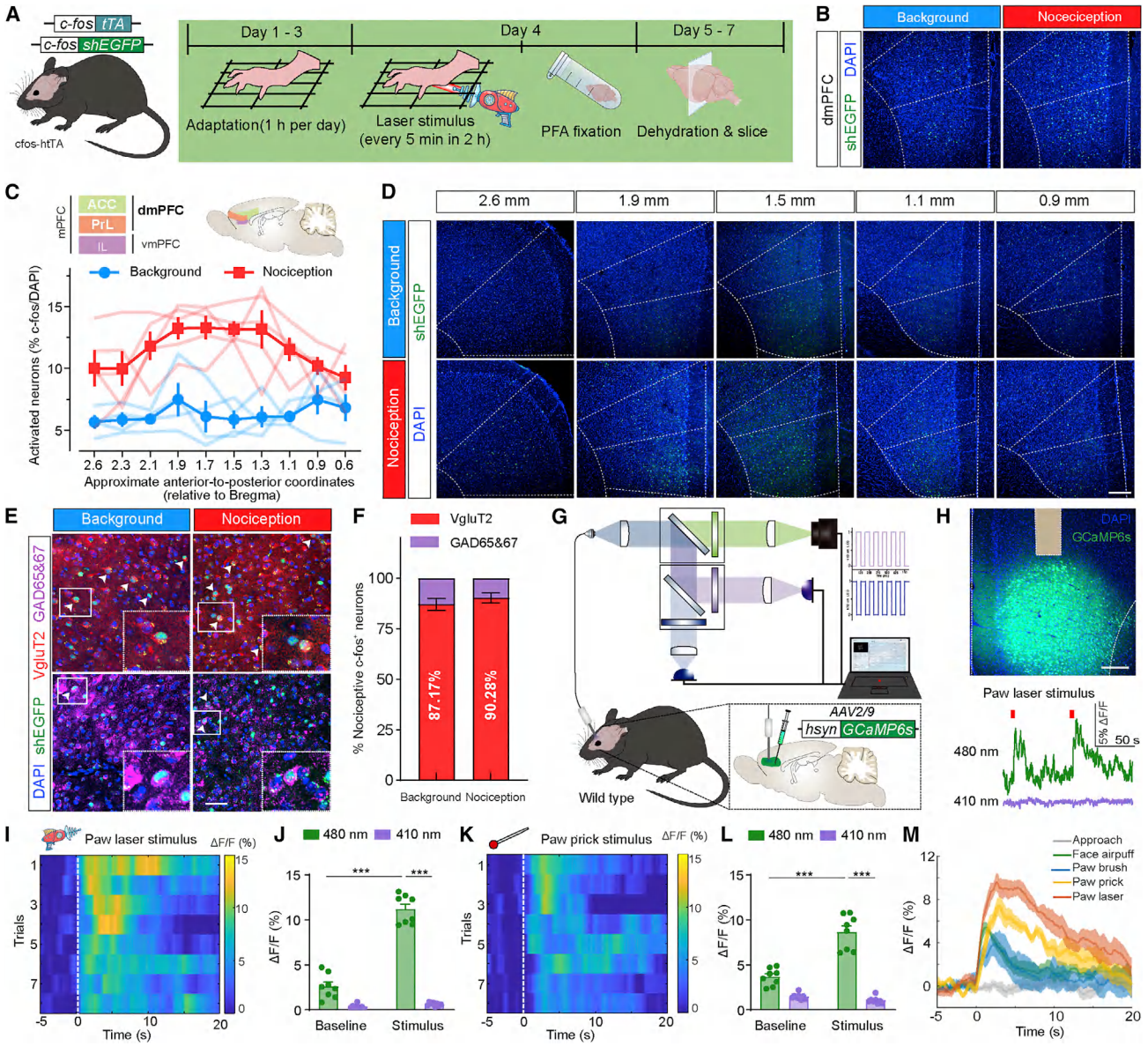

Figure 1. A neuronal ensemble in dmPFC activated upon acute hind paw nociceptive stimuli

(A) Left: A cartoon mouse illustrating the transgenic components. Right: Experimental scheme for hind paw laser stimuli-induced neuronal activities screening using cfos-htTA transgenic mice.

(B) Confocal images of shEGFP$^+$ cells in dmPFC of Nociception and Background groups. Nuclei in blue (DAPI). Scale bar, 200 μm.

(C) Top: Schematic for definition and localization of dmPFC. Bottom: Anterior to posterior axis quantification of the number of shEGFP$^+$ neurons in dmPFC induced by hind paw laser stimuli (n = 4 mice for either group).

(D) Confocal images of shEGFP$^+$ cells in dmPFC showing anterior to posterior distribution pattern of neuronal activities induced by peripheral nociceptive stimuli. Nuclei in blue (DAPI). Scale bar, 200 μm.

(E) Confocal images of glutamatergic (anti-VgluT2, red) and GABAergic (anti-GAD 65&67, purple) neurons in dmPFC nociception- and background-labeled neurons via immunostaining. White arrowheads indicate double-positive neurons. White rectangle areas were magnified in insets. Scale bar, 50 μm.

(F) Percentage of VGlut2 positive (red) and GAD67 positive (purple) among nociception- or background-labeled dmPFC neurons (n = 3–4 mice, two-way ANOVA with Bonferroni's post hoc test). Nuclei in blue (DAPI).

(G) Schematic for AAV2/9-hSyn-GCaMP6s injection of wild-type mice and fiber photometry recording in the dmPFC.

(H) Top: confocal images showing the expression of AAV2/9-hSyn-GCaMP6s virus (green) and the track of optical fiber in dmPFC. Nuclei in blue (DAPI). Scale bar, 200 μm. Bottom: raw traces of signal excited by 480 nm (green) and 410 nm (purple) upon paw laser stimulus. Red bars indicate paw laser stimulus (5 ms).

(I) Heatmap showing the response of dmPFC neurons to hind paw laser stimuli, with each row representing the response of one trial. White broken line indicates time of the stimulus.

(legend continued on next page)

Such discrepancies may stem from the fact that the dmPFC is composed of different neuronal subpopulations with distinct morphologic, anatomic, physiological, and functional features, which differentially contribute to pain modulation. In the present study, we identified a nociceptive neuronal ensemble in the dmPFC that showed prominent excitatory reactivity to nociceptive stimuli and actively contributed to the development of chronic pain.

RESULTS

A neuronal ensemble in dmPFC shows prominent activation upon acute nociceptive stimuli

To investigate how pain signals were processed in the brain, we used cfos-htTA mice, which expressed 2-hour half-life green fluorescent protein (shEGFP) and tetracycline transcriptional activator (tTA) under the control of the cfos promoter, to examine the activation pattern of neuronal ensembles in the classic pain matrix upon nociceptive laser stimuli delivered to the hind paw (Figure 1A). The power of the laser was sufficient to induce nociceptive responses but not prolonged allodynia in mice, confirmed from a pilot test (Figures S1A–S1D).

We observed significant increases in the portion of activated neurons in the dmPFC, as well as some other regions, such as the hind leg region of somatosensory cortex (S1HL) and the basolateral amygdala (BLA) (Figures 1B, S1E, and S1F), consistent with previous studies.[24–26] As dmPFC consisted of PrL and rACC, we further examined the distribution pattern of laser-activated neurons in the dmPFC along the anterior-posterior axis. We found that most cfos-positive neurons in the dmPFC located at coronal planes ranging from 2.1 to 1.1 mm relative to bregma, broadly spreading from superficial to deep layers (Figures 1C and 1D). We did not observe significant lateralization of dmPFC responses to ipsi- or contralateral hind paw stimuli (Figure S1G). Furthermore, most (90.3% ± 2.4%) cfos-positive neurons in response to nociceptive laser stimuli were found to be co-labeled with vesicular glutamate transporter type 2 (VGlut2, a marker of glutamatergic neurons), while only a small proportion (9.7% ± 2.4%) with glutamic acid decarboxylase 65 and 67 (GAD65&67, markers of GABAergic neurons). No significant difference in the portion of VGlut2 and GAD65&67 in cfos-labeled dmPFC neurons was found between background (87.2% ± 2.9% for VGlut2 and 12.8% ± 2.9% for GAD65&67, respectively) and nociception groups (Figures 1E and 1F).

To further confirm dynamic changes in the activity of dmPFC neurons in response to noxious stimuli, we used *in vivo* fiber photometry to monitor Ca^{2+} signal fluctuation. AAV2/9-hSyn-GCaMP6s was injected and optical fiber was implanted into the right dmPFC (Figures 1G, 1H, and S1H). We found that dmPFC neurons were activated by noxious thermal stimuli delivered onto either side of hind paw, as evidenced by significant elevation of fluorescent signals excited by 480 nm (Figures 1I and 1J), while no significant fluorescent signals fluctuation was observed under 410 nm, excluding the influence from locomotion during recording (Figure 1J). Besides, prominent responses of dmPFC neurons were also observed to mechanical stimuli (prick) applied to the hind paw (Figures 1K and 1L). By contrast, these neurons showed much less activation by aversive facial stimuli (airpuff) or non-nociceptive tactile stimuli (brush) onto the hind paw (Figures 1M and S1I–S1L). Together, these results reveal a neuronal ensemble in the dmPFC showing prominent activation upon acute nociceptive stimuli.

Increased activity of the dmPFC nociceptive ensemble to noxious stimuli under chronic inflammatory pain

Next, to investigate the real-time reactivity of dmPFC to external stimuli under chronic pain condition at the single neuronal level, we used *in vivo* miniaturized two-photon recording in freely behaving mice before and after hind paw CFA injection (Figures 2A–2C and S2A).

Under baseline conditions, noxious pin prick and laser stimuli induced significant Ca^{2+} responses in 12.9% and 12.8% dmPFC neurons, respectively. Here we regarded principal neurons that responded to either noxious pin and/or noxious laser as the dmPFC nociceptive ensemble. Still, mild hind paw touch induced responses in about 7.9% of neurons (Figures 2D and 2E). Under inflammatory pain, a larger portion of dmPFC neurons responded to noxious stimuli (Figures 2D and 2E); 21.3% and 19.1% of dmPFC neurons responded positively to noxious pin prick and laser, respectively, on day 1 following hind paw CFA injection (Figure 2E). The proportion of activated dmPFC neurons gradually decreased at later stages of inflammatory pain (days 3–9) along with the recovery from allodynia (Figures 2F, S2B, and S2C). A similar trend was observed with tactile stimuli (Figure 2F). Importantly, long-term tracking of the dmPFC neuronal ensemble revealed that a subset of nociceptive neurons (27% of the 274 cross-day-aligned nociceptive neurons) maintained their nociceptive properties for at least 10 days after CFA injection (Figures S2D and S2E), suggesting that this neuronal ensemble might be actively involved throughout the development of inflammatory pain.

Moreover, the reactivity of dmPFC neurons to noxious prick and laser, but not innoxious touch, also significantly increased in inflammatory pain (Figures 2G–2J). Meanwhile, the frequency, rather than the peak, of spontaneous activity among the overall dmPFC population and nociceptive ensemble significantly decreased in inflammatory pain (Figures S2F–S2K). One crucial finding was that stronger activation of the dmPFC nociceptive

(J) Quantification of GCaMP6s signal in dmPFC neurons evoked by hind paw laser stimuli (n = 4 mice, two trials from each mouse, two-way ANOVA with Bonferroni's post hoc test).
(K) Heatmap showing the response of dmPFC neurons to hind paw prick stimuli, with each row representing the response of one trial. White broken line indicates time of the stimulus.
(L) Quantification of GCaMP6s signals in dmPFC neurons evoked by hind paw prick stimuli (n = 4 mice, two trials from each mouse, two-way ANOVA with Bonferroni's post hoc test).
(M) Average temporal GCaMP6s signal in dmPFC neurons evoked by approach (gray), face airpuff (green), paw brush (blue), paw prick (yellow), and paw laser stimulation (red) (n = 4 mice). *$p < 0.05$, **$p < 0.01$, and ***$p < 0.001$. Data are represented as mean ± SEM, and shaded areas indicate SEM. See also Figure S1.

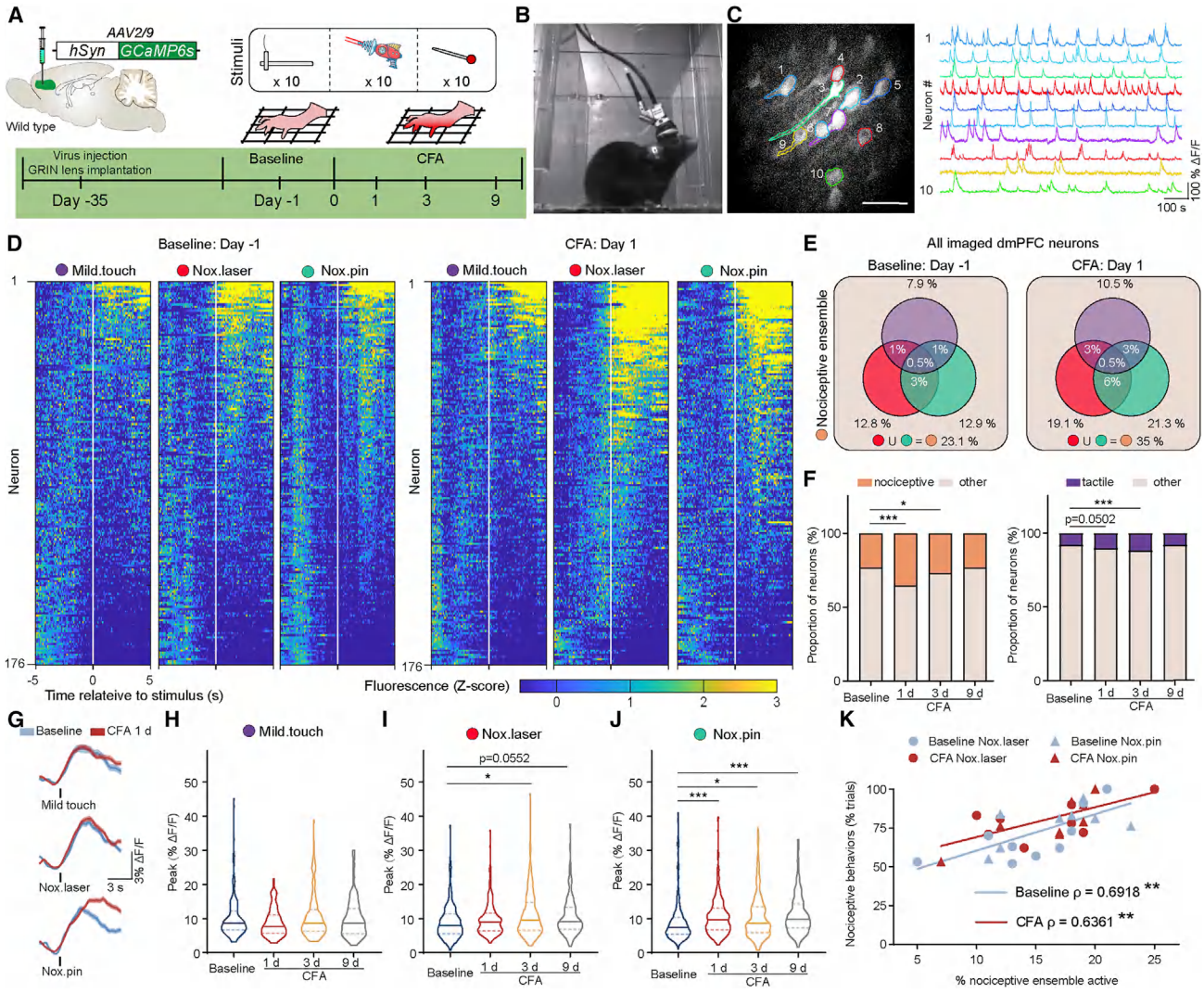

Figure 2. Two-photon recording of dmPFC neurons in CFA-induced inflammatory pain

(A) Top left: Schematic showing AAV2/9-hSyn-GCaMP6s virus (green) injected into the unilateral dmPFC of wild-type mice. Top right: Schematic diagram of stimuli strategy before and after CFA injection. Bottom: Experimental scheme for virus injection, stimuli, and recording.

(B) An example image of two-photon recording.

(C) Left: Image of dmPFC neurons expressing GCaMP6s. Exampled neurons are outlined in different colors. Right: Corresponding representative calcium traces from 10 neurons of interest (color-matched to the left). Scale bar, 100 μm.

(D) Mean Ca^{2+} activity (Z-scored ΔF/F) of all neurons from the same mouse for that imaging session, before (left) and after (right) paw CFA injection, in response to mild touch stimuli, noxious laser, and noxious pin prick. Neurons were sorted for each stimulus by average responses in 5-s post stimulus onset.

(E) Venn diagram of neuronal populations in response to mild touch stimuli, noxious pin prick, and noxious laser before (left) and after (right) paw CFA injection. Numbers show means of percentages of significantly responsive neurons. Nociceptive ensemble is a global cell that responded to either noxious pin and/or noxious laser (Baseline: n = 1,341 neurons from nine mice; CFA 1 d: n = 1,203 neurons from eight mice).

(F) Left: Percentages of nociceptive ensemble at baseline, CFA 1 d, 3 d, and 9 d after paw CFA injection. Right: Percentages of neurons responding to mild touch stimuli at baseline, CFA 1 d, 3 d, and 9 d after paw CFA injection (Baseline, 1 d, 3 d: n = 1,341 neurons from nine mice; 9 d: n = 1,203 neurons from eight mice, chi-square test).

(G) Mean Ca^{2+} activity within the neurons responding to mild touch (top), noxious pin laser (middle), and noxious pin prick (bottom).

(H–J) Peak Ca^{2+} activity of neurons responding to mild touch (H), noxious laser (I), noxious pin prick (J) stimuli at baseline, 1 d, 3 d, and 9 d after paw CFA injection. Data are represented as median, quartiles, and min to max (Baseline, 1 d, 3 d: n = 1,341 neurons from nine mice; 9 d: n = 1,203 neurons from eight mice, Kruskal-Wallis test with Dunn's post hoc test).

(K) Spearman's correlations between average percentage of nociceptive ensemble activation per trial and percentage of nociceptive responses across stimulus and conditions. *p < 0.05, **p < 0.01, and ***p < 0.001. Data, except for (H–J) are represented as mean ± SEM, shaded areas indicate SEM. See also Figure S2.

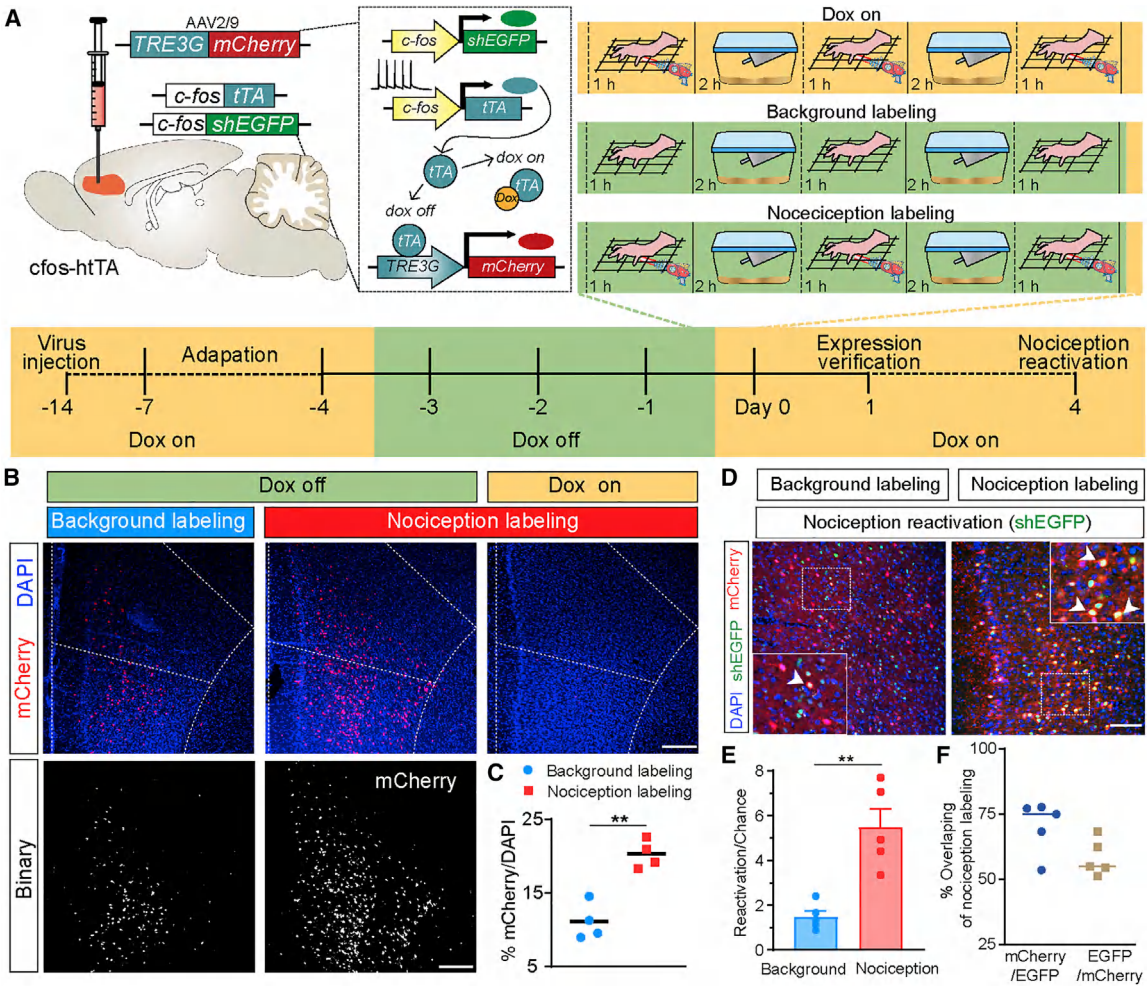

Figure 3. Labeling nociceptive neurons in the dmPFC via the Tet-off system

(A) Top left: Schematic showing AAV2/9-TRE3G-mCherry injection into bilateral dmPFC of cfos-htTA mice. Top middle: Schematic diagram of Tet-off system. Top right: Experimental strategy to label the activated neurons upon nociceptive stimuli, with background labeling or dox-always-on as control groups. Bottom: Experimental scheme for virus injection, dox switching, activated neurons labeling, expression verification, and nociception reactivation.

(B) Top: Confocal images of mCherry$^+$ (red) cells in dmPFC labeled by nociceptive stimuli or background under dox-off or dox-always-on. Nuclei in blue (DAPI). Bottom: Confocal images of mCherry$^+$ cells (white) in binary mode corresponding to images above. Scale bar, 200 μm.

(C) Percentage of mCherry$^+$ cells in the dmPFC in background- and nociception-labeling groups (n = 4 mice, unpaired Student's t test).

(D) Confocal images of nociception reactivation cells (shEGFP$^+$) in the dmPFC labeled by nociception stimuli or background (mCherry$^+$). White arrowheads indicate double-positive cells. White rectangle areas are magnified in insets. Scale bar, 100 μm.

(E) Quantification of reactivated cells (shEGFP$^+$) by nociceptive stimuli among nociception- or background-labeled neurons (mCherry$^+$), normalized by chance level (n = 5 mice, unpaired Student's t test).

(F) Overlaying percentage of reactivated cells (shEGFP$^+$) by nociception stimuli in nociception stimuli-labeled neurons (mCherry$^+$) and inverse percentage (n = 5 mice). *p < 0.05, **p < 0.01, and ***p < 0.001. Data are represented as mean ± SEM.

ensemble was predictive of increased nociceptive behaviors, suggesting correlated dmPFC nociceptive processing and the magnitude of pain behaviors (Figure 1K).

A Tet-off system for selectively identifying nociception-activated neurons in dmPFC

To identify and further manipulate the neuronal ensemble in dmPFC reactive to nociception, AAV2/9-TRE3G-mCherry was injected into the dmPFC of cfos-htTA transgenic mice. In this Tet-off system, dmPFC cells activated during paw laser stimuli (5 ms of duration and 4–6 W of power) would express mCherry in the absence of doxycycline (dox) under the dual control of the cfos promoter and tTA. Moreover, shEGFP, designed to share a similar degradation pattern to cfos, allowed tag of activated neurons induced by nociceptive stimuli given before mice were killed (Figure 3A).

To characterize the inducibility and activity-dependence of mCherry expression, two groups of mice were exposed to the same context with (nociception labeling) or without (background labeling) hind paw stimuli following 3 days' dox-off (Figure 3B).

Notably, nociceptive stimuli resulted in nearly twice the proportion of mCherry$^+$ cells in the dmPFC compared with background labeling (Figure 3C).

Next, we tested the reactivation efficiency of the dmPFC ensemble labeled by the system (mCherry-positive) via delivering nociceptive stimuli again on day 4 following dox re-treatment, when neurons activated by subsequent stimuli expressed shEGFP driven by cfos promoter (Figure 3D). The reactivation rate of mCherry$^+$ cells was assessed via dividing the percentage of shEGFP$^+$ and mCherry$^+$ double-positive cells among DAPI by chance level [(shEGFP$^+$/DAPI) × (mCherry$^+$/DAPI)]. We found that, in mice with nociceptive stimuli, the reactivation rate of the dmPFC ensemble was significantly higher compared with the background group (Figure 3E), and most of shEGFP$^+$ cells were mCherry$^+$ though not all mCherry$^+$ cells expressed shEGFP (Figure 3F). Taken together, these results suggest that nociception-activated neurons in the dmPFC could be labeled by the Tet-off system.

Molecular and efferent features of nociception-labeled neurons in dmPFC

If the nociceptive neuronal ensemble in the dmPFC contributed to pain chronicity, we hypothesized that these neurons would show molecular and efferent characteristics closely related to pain modulation. To test this hypothesis, we first performed fluorescence-activated cell sorting (FACS) and transcriptome sequencing via Smart-Seq2 (Figures 4A and S3A). Compared with background-labeled ensemble, a total of 890 of 25,186 genes were identified to show statistically higher expression (orange) (take 2 as the threshold of fold change), including *Htr1f*, *Oprl1,* and *Cdk3*, which were reported to be involved in pain signal processing.[17,27,28] Besides, a total of 296 of 25,186 genes showed statistically lower expression (blue) in nociception-labeled neurons (Figure 4B). Meanwhile, gene ontology (GO) enrichment analysis indicated that up-regulated genes were most prominently engaged in biological processes of G protein-coupled receptor signaling, sensory perception, and detection of stimulus (Figures 4C and S3B–S3D).

Next, we used antegrade transneuronal AAV2/1-hSyn-Cre and Ai9 mice to trace the downstream projections of dmPFC neurons (Figure 3D), and we found multiple potential downstream targets of dmPFC neurons including insular cortex (IC), nucleus accumbens core (AcbC), BLA, PAG, and lateral parabrachial nucleus (LPB), etc. (Figures 4E, 4F, S4A, and S4B). Many of these regions are actively involved in processing sensory or emotional aspects of pain.[20,25,29]

To further confirm the connectivity, we injected retrograde AAV2/Retro-hSyn-mCherry into bilateral BLA, PAG, LPB, and AcbC, the four potential downstream targets of dmPFC nociceptive neurons involved in sensory or emotional aspects of pain, of cfos-htTA transgenic mice. Three weeks after virus injection when retrograde-traced neurons in dmPFC expressed mCherry, mice received paw laser stimuli to tag nociception-activated neuron (shEGFP$^+$) (Figure 4G). We observed that 18.3% of dmPFC nociceptive neurons projected to BLA, 15.7% to AcbC, 15.3% to PAG, and only 1.1% to LPB. Moreover, we found that dmPFC nociceptive neurons projecting to AcbC mostly located at layer 2/3, neurons projecting to PAG and LPB were almost all from layer 5 of dmPFC, while those projecting to BLA were from both layer 2/3 and layer 5 (Figures 4H–4J and S4C). Together, these results suggest that dmPFC nociceptive neurons exhibit molecular and efferent features indicative of active pain processing.

Prolonged artificial activation of dmPFC nociception-labeled neurons induced chronic pain-like behaviors in normal mice

We next directly tested whether artificial activation of the dmPFC nociception-activated neuronal ensemble could induce chronic pain-like behaviors. cfos-htTA transgenic mice were injected with AAV2/9-TRE3G-hM3DGq-mCherry into the dmPFC, and AAV2/9-TRE3G-mCherry virus was injected as control (Figures 5A and S5A). The nociceptive neuronal ensemble in dmPFC was tagged and selectively activated by the administration of Clozapine N-oxide (CNO, Figure 5B).

We found that chemogenetic activation of dmPFC nociception-activated neuronal ensemble for 6 consecutive days (twice per day) induced significant thermal hyperalgesia and mechanical allodynia in normal mice, which persisted even 1 week after termination of CNO administration (Figures 5C and 5D). We also recorded spontaneous behaviors of mice during CNO administration. Though we did not observe significant changes in the time of grooming or paw licking and flinching (Figures S5B–S5D), dmPFC nociceptive neuronal activation significantly increased mice preference to an analgesic dose (1 mg kg^{-1}) of morphine-paired chamber in the conditioned place preference (CPP) test on days 4–5 but not days 10–11 post CNO administration (Figures 5E–5G and S5E).

On days 10–11, mice with dmPFC nociceptive neuronal activation also showed significantly increased level of anxiety (Figures 5H–6Q). It should be noted that such anxiety-like behaviors were not observed at an earlier phase (days 3–4) during CNO administration when mice already showed hyperalgesia and allodynia in response to dmPFC ensemble activation (Figures S5F–S5K). These results indicate that the dmPFC ensemble activation-induced hyperalgesia and allodynia are not results but incentives of anxiety-like behaviors.

Interestingly, pan activation of randomly transfected dmPFC pyramidal neurons (Figures S6A and S6B), using CamKII-hM3DGq-mCherry in combination with CNO, did not induce hyperalgesia or allodynia (Figures S6C and S6D), nor preference to morphine-paired chamber for spontaneous pain test (Figures S6E and S6F) or anxiety-like behaviors (Figures S6G–S6N), suggesting that the chronic pain-like behaviors were specifically induced by prolonged activation of the nociceptive ensemble in the dmPFC, but not the entire dmPFC.

Prolonged artificial activation of dmPFC nociception-labeled neurons up-regulated neuronal activity and responses to peripheral noxious stimuli of BLA and LPB

We next explored whether long-term artificial activation of nociceptive dmPFC neurons would induce chronic pain-like activity patterns of the downstream regions. Consistent with previous findings that neurons showed excitatory and inhibitory spontaneous current adaptation in response to prolonged chemogenetic activation,[30,31] we found that, after consecutive 6 days' (twice per day) CNO-induced activation (Figures 6A and 6B), the excitability of dmPFC nociceptive pyramidal neurons was

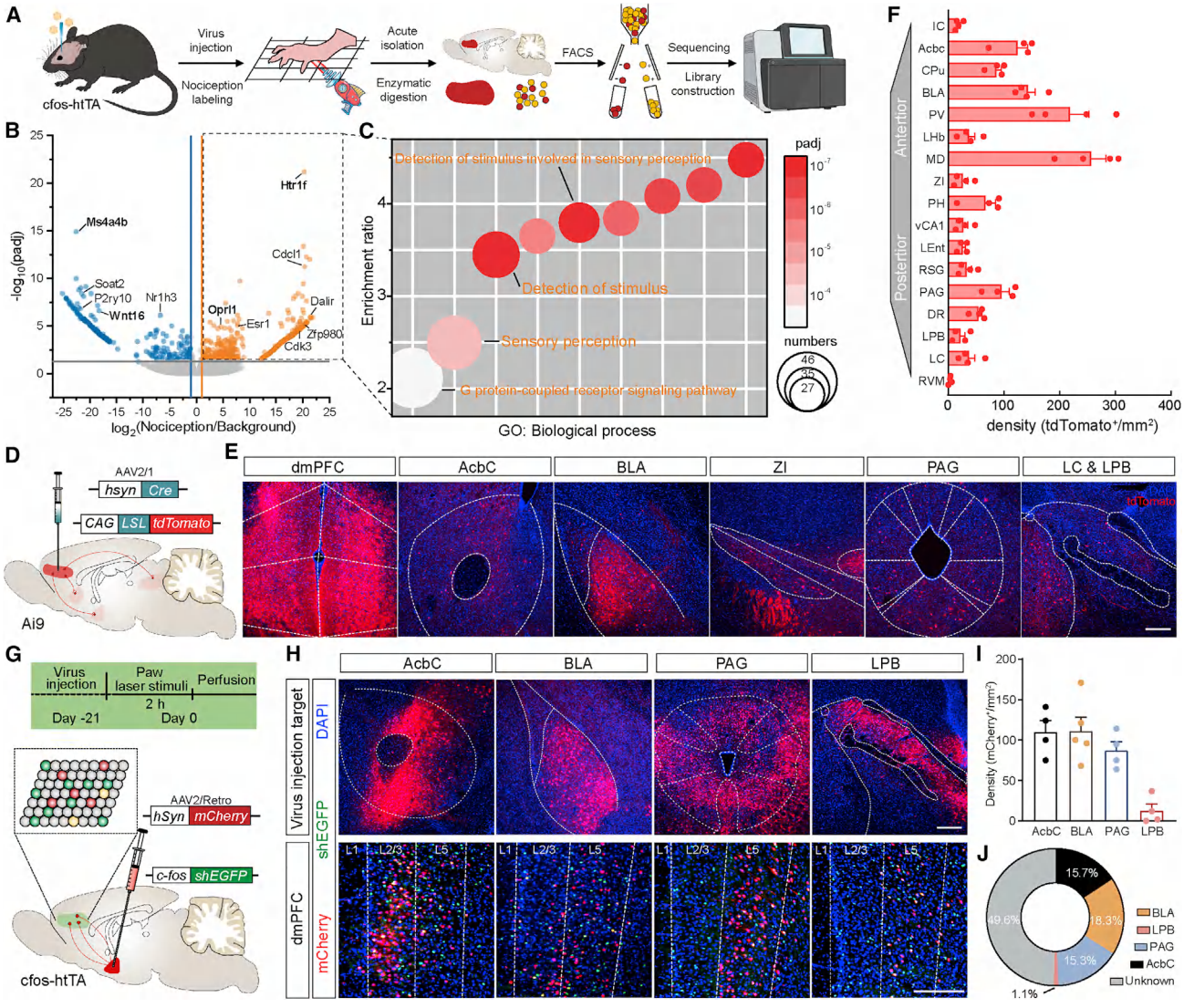

Figure 4. Molecular and efferent features of the nociceptive neuronal ensemble in the dmPFC

(A) Flowchart showing purification of mCherry$^+$ neurons from brain of cfos-htTA mice after nociception or background label via FACS.

(B) Volcano plot showing 890 of 25,186 genes were statistically high-expressed (orange) while 296 of 25,186 genes were statistically low-expressed (blue) in nociceptive neurons, compared with background-labeled ensemble (n = 4 mice for either group, Benjamini-Hochberg adjusted p value was used).

(C) Biological processes in gene ontology (GO) enrichment analysis of different expressed genes between nociception and background-labeled neurons via g:Profiler (Benjamini-Hochberg adjusted p value was used).

(D) Schematic showing AAV2/1-hSyn-Cre injection into bilateral dmPFC of Ai9 mice.

(E) Confocal images of mCherry$^+$ cells in dmPFC, AcbC, BLA, ZI, PAG, LC, and LPB. Nuclei in blue (DAPI). Scale bar, 200 μm.

(F) Quantification of mCherry$^+$ cells across 17 brain regions, normalized by corresponding area (n = 4 mice).

(G) Top: Experimental scheme for virus injection, paw laser stimuli, and perfusion. Bottom: Schematic showing AAV2/Retro-hSyn-mCherry injection into bilateral AcbC, BLA, PAG, and LPB of cfos-htTA mice.

(H) Upper panel: Confocal images of mCherry$^+$ cells in AcbC, BLA, PAG, and LPB *in situ*. Lower panel: Confocal images of retrograde virus (mCherry$^+$) and nociception-activated neurons (shEGFP$^+$) in dmPFC. Nuclei in blue (DAPI). Scale bar, 200 μm.

(I) Quantification of mCherry$^+$ cells in dmPFC retrograding from AcbC, BLA, PAG, and LPB, normalized by corresponding area (n = 4–5 mice).

(J) Percentage of downstream projection of dmPFC nociceptive neurons (n = 4–5 mice). *p < 0.05, **p < 0.01, and ***p < 0.001. Data are represented as mean ± SEM. See also Figures S3 and S4.

significantly enhanced (Figures 6C and 6D) and a detailed input (current injection)/output (number of action potentials [AP]) curve in response to a stepped depolarizing current drawn for both groups of mice (Figure 6D).

To further understand the specific downstream projection targets of dmPFC nociceptive neurons, AAV2/9-TRE3G-hM3DGq-mCherry was injected into the dmPFC of cfos-htTA transgenic mice and CNO was used for 6 consecutive days to repeatedly

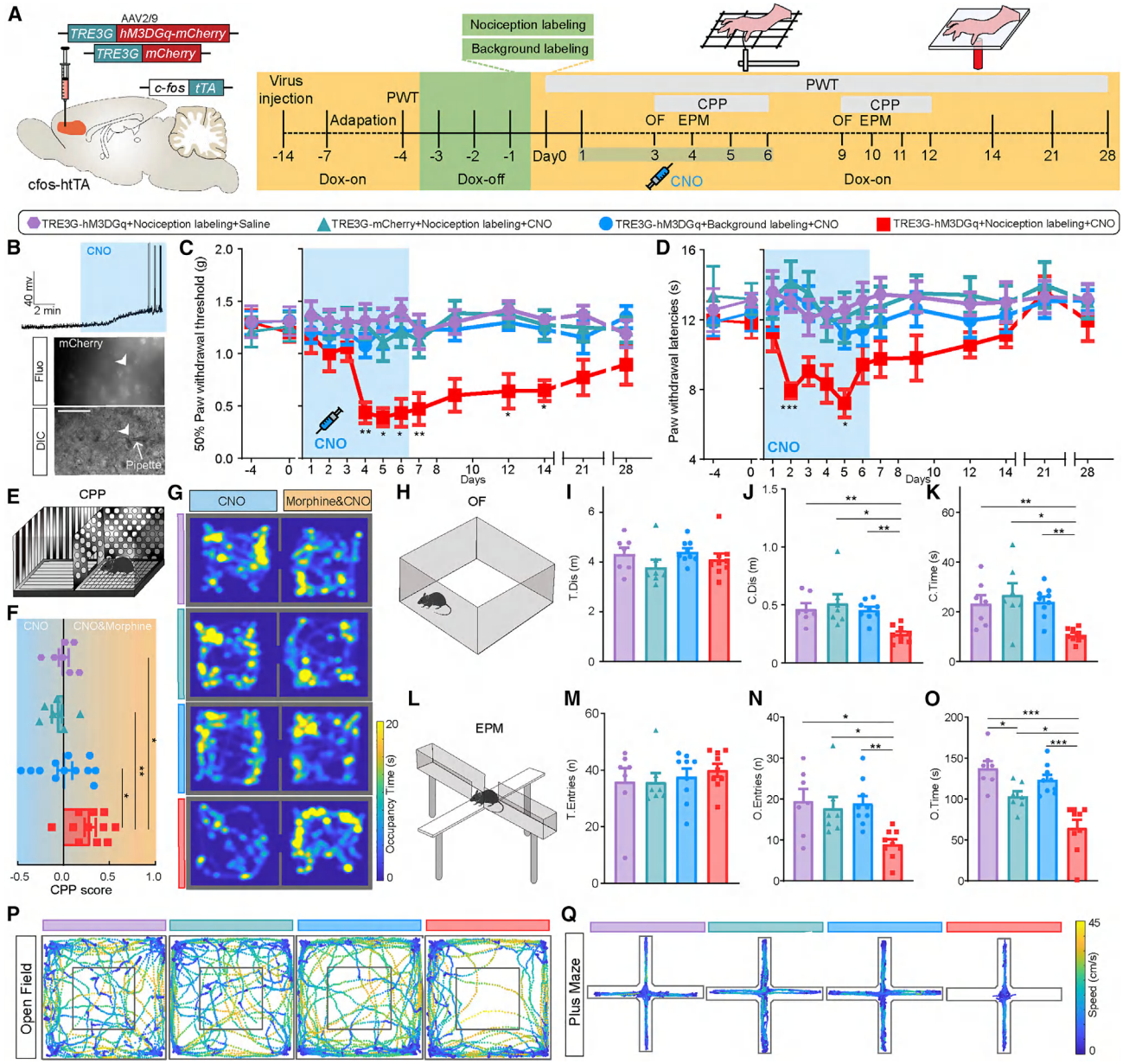

Figure 5. Prolonged artificial activation of dmPFC nociceptive neurons induces chronic pain-like behaviors

(A) Left: Schematic showing AAV2/9-TRE3G-hMDGq-mCherry or AAV2/9-TRE3G-mCherry injection into the bilateral dmPFC of cfos-htTA mice. Right: Experimental scheme for virus injection, dox switching, activated neurons labeling, CNO administration and behavioral tests. CNO was administrated (1 mg kg^{-1}, intraperitoneal) during day 1–6 twice per day. Paw withdrawal threshold (PWT) was measured on days −4, 0, 1, 2, 3, 4, 5, 6, 7, 9, 12, 14, 21, and 28. Conditioned place preference (CPP) was measured during days 3–6 and days 9–12. Open field (OF) and elevated plus maze (EPM) were measured on days 4–5 and days 10–11, respectively.

(B) Top: Whole-cell current-clamp recording from hM3DGq expressed dmPFC neurons with bath application of 10 μM CNO (blue shade). The experiment was independently repeated in four neurons from two mice, with similar results obtained. Bottom: Fluorescent (upper) and infrared differential interference contrast (lower) images of hM3DGq-mCherry expressed dmPFC neurons. White arrowhead indicates $mCherry^{+}$ cell recorded by glass electrode. Scale bar, 20 μm.

(C and D) Mechanical paw withdrawal thresholds (C) and thermal paw withdrawal latencies (D) in mice during prolonged artificial activation of dmPFC nociceptive neurons (n = 7–11 mice, two-way repeated measure ANOVA with Bonferroni's post hoc test).

(E) Cartoon illustrating the structure of the CPP box.

(F) CPP score of mice expressing mCherry or hM3DGq-mCherry in nociception- or background-labeled neurons after analgesic dose (1 mg kg^{-1}) of morphine conditioning measured on days 3–6 (n = 7–12 mice, one-way ANOVA with Bonferroni's post hoc test).

(G) Heatmap of CPP test session, color coded for the relative occupancy time.

(H) Cartoon showing the structure of the open field (OF).

(legend continued on next page)

activate nociceptive neurons in the dmPFC (Figure 6E). We observed that, shortly after the last CNO administration, most prominent increases in the number of active neurons (shEGFP$^+$) were found in BLA, CeA, ventrolateral PAG (vlPAG), and LPB, compared with the background labeling group (Figures 6F and 6G).

Consistently, by recording calcium signals in downstream brain areas at baseline, day 1 and day 7 following CNO administration (Figures 6H, 6I, and S7A), we found that chemogenetic activation of dmPFC nociceptive neurons increased the response of BLA neurons upon paw laser stimuli but not at background labeling group on both days 1 and 7 post CNO (Figures 6J, 6K, S7B, and S7C). Similarly, activation of dmPFC nociceptive neurons also increased the response of LPB calcium signals upon paw laser stimuli on day 7 post CNO (Figures 6L, 6M, S7D, and S7E). However, we did not observe any changes in vlPAG calcium signals (Figures 6N, 6O, S7F, and S7G). Intriguingly, the activity changes of BLA and LPB mimicked those observed under CFA-induced chronic pain (Figures S7H–S7M), further indicating the possible involvement of this nociceptive dmPFC ensemble in pain chronicity.

Long-term suppression of dmPFC nociceptive neurons relieved chronic inflammation pain

Finally, to determine the necessity of the dmPFC nociceptive ensemble in chronic pain development, we injected AAV2/9-TRE3G-hM4DGi-mCherry into the dmPFC of cfos-htTA mice (Figure 7A). Thus, the nociception-activated dmPFC ensemble could be tagged as well as suppressed through the administration of CNO (Figure 7B).

We found that long-term chemogenetic suppression of the nociception-activated neuronal ensemble in dmPFC significantly ameliorated CFA-induced thermal hyperalgesia and mechanical allodynia, but did not affect saline-treated normal mice (Figures 7C and 7D). Meanwhile, chemogenetic suppression also decreased spontaneous pain behaviors, including grooming, paw licking, and paw filching during 2–3 days post-CFA injection (Figures 7E–7G, Videos S1 and S2). The analgesic effect of dmPFC ensemble inhibition on longitudinal timing of spontaneous pain was further confirmed in the CPP test, in which mice with inflammatory pain spent more time in the CNO-paired chamber after conditioning during 2–4 days post-CFA injection (Figures 7H and 7I). Chemogenetic suppression of the dmPFC ensemble also significantly decreased pain-associated anxiety-like behaviors in mice, as indicated by more time spent (C.Time) and distance traveled (C.Dis) in the central area of the open field (Figures 7J–7M), as well as more time spent (O.Time) and entries (O.Entries) into the open arms of the elevated plus maze (Figures 7N–7Q). Together, these findings suggest that suppressing the nociceptive dmPFC neuronal ensemble attenuates chronic inflammatory pain.

DISCUSSION

Identification of a nociception-responsive neuronal ensemble in dmPFC

Although it is well-known that the morphology and function of dmPFC are reorganized in chronic pain,[9,10,17,32,33] whether different dmPFC subpopulations play distinct roles in this process is poorly defined. We identified here a specific neuronal ensemble in dmPFC responsive to peripheral noxious stimuli via cfos screening and *in vivo* fiber photometry. Indeed, it was also evidenced in rats that mPFC showed increased responses to peripheral noxious stimulations.[24] The present study has revealed significantly increased responsive proportion and elevated peak response of the dmPFC nociceptive ensemble in inflammatory pain (Figures 2F, 2I, and 2J). While our results are in line with previous studies showing increased mPFC activity in chronic pain patients[7,8] and rodents,[9,10,34] others have reported contradictory findings. Decreased intrinsic excitability and firing rates of mPFC neurons have been reported.[24] These findings indicate functional variations among different dmPFC neuronal ensembles in pain.

Distinct molecular feature and functional connectivity of dmPFC nociceptive ensemble

We genetically labeled the dmPFC nociceptive neurons showing positive responses to peripheral nociceptive stimuli. Through transcriptome analysis, we found genes highly expressed in this dmPFC nociceptive ensemble compared with background tagged neurons, including Oprl1, Htr1f, and several olfactory receptors (Figure 4B). Oprl1 is known as the nociceptin/orphanin FQ receptor, whose effect on the central nervous system can be either similar or opposite to opioids in a location-dependent manner.[35] Htr1f, the F subtype of serotonin receptor 1, has also been discovered related to abnormal pain threshold.[28] We also found several olfactory receptors highly expressed in dmPFC nociceptive ensemble (Figures S3C and S3D). This was unlikely resultant from contamination from olfactory bulbs, which were carefully resected in both background- and nociception-labeling groups. Indeed, olfactory receptors are widely expressed in non-sensory brain regions, including the cerebral cortex and limbic system, and exert functions unrelated to olfaction.[36,37] These molecular characteristics support contribution of this nociceptive ensemble in pain modulation. Although researchers have found excited or suppressed neuronal activities in the mPFC from different behavioral paradigms, so far there is little evidence

(I–K) Quantification of total distance (T.Dis) traveled in the field (I), distance traveled (C.Dis) in the central area (J), and time spent (C.Time) in the central area (K) in the open field test measured on day 9 (n = 7–9 mice, one-way ANOVA with Bonferroni's post hoc test).
(I) Cartoon showing the structure of the elevated plus maze (EPM).
(M–O) Quantification of total arm entries (T.Entries) (M), numbers of entries (O.Entries) into open arms (N), and time spent (O.Time) in open arms (O) in elevated plus maze test measured on day 10 (n = 7–9 mice, one-way ANOVA with Bonferroni's post hoc test).
(P) Exploratory heat traces in the open field (OF), color coded for the movement speed.
(Q) Exploratory heat traces in the elevated plus maze (EPM), color coded for the movement speed. *$p < 0.05$, **$p < 0.01$, and ***$p < 0.001$. Data are represented as mean ± SEM. See also Figures S5 and S6.

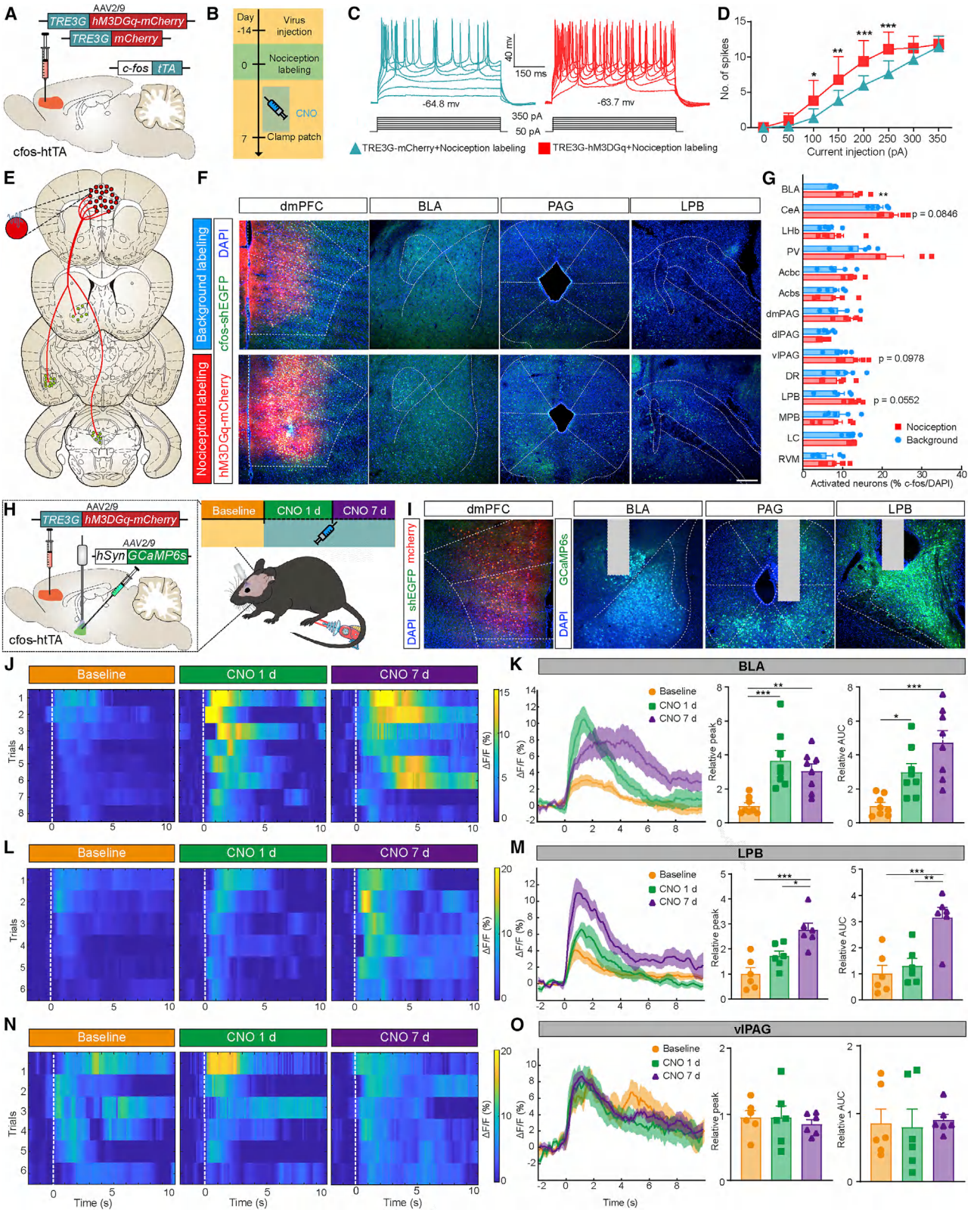

(legend on next page)

regarding whether the responsive neuronal ensemble shows specific gene markers.[38–40] By contrast, specific molecular characteristics have been found in distinct subsets of BLA neurons that encode antagonistic negative and positive representations.[41] Thus, further validating work will be needed to delve into more specific information of those neuronal ensembles in the dmPFC.

dmPFC nociceptive neurons exhibit enhanced excitability after consecutive 6 days' CNO-induced activation (Figures 6C and 6D). Although this ensemble is heterogeneous, more than 90% of them are glutamatergic excitatory neurons. Considering that parvalbumin-expressing interneurons are less likely to express immediate-early genes (IEGs), including cfos,[42] we focused more on nociceptive pyramidal neurons. In the present study, electrophysiological recording on nociceptive pyramidal neurons was performed in a non-synaptically isolated paradigm, and in consequence, it would be hard to distinguish whether the increase in neuronal activity was mediated by altered synaptic inputs in microcircuitry, or a change in intrinsic neuronal activity. However, there is evidence for both enhanced functional connectivity after recurrent optogenetic coactivation of a neuronal group and altered gene expressions, as well as excitatory and inhibitory spontaneous currents with chronic chemogenetic manipulation of neurons.[31,43,44] Hence, the increase in neuronal activity in our study may be mediated by both altered synaptic inputs and changed intrinsic activity, which does not affect our conclusion of increased activity of neuronal ensemble as the result of 6-day CNO administrations.

Based on our dmPFC neuron anterograde tracing results (Figures 4D–4F and S4A), as well as previous work on dmPFC connectivity[45–47] and the pain matrix,[20,25,29,48–50] we selected AcbC, BLA, PAG, and LPB for retrograde tracing to the dmPFC nociceptive ensemble (Figures 4G–4J). Interestingly, except for LPB (1.1%), the dmPFC nociceptive ensemble displayed even projection to all three regions (AcbC, 15.7%; BLA, 18.3%; PAG, 15.3%). Based on the fact above, we combined downstream cfos screening and fiber photometry recording in potent brain regions and found that BLA and LPB showed elevated neuronal activity and response to peripheral noxious stimuli, exactly as observed under chronic pain conditions. We noticed that long-term mPFC nociceptive ensemble activation was necessary for the responses of LPB. A possible explanation is that dmPFC regulates LPB activity through multistage projections, for example dmPFC – BLA – CeA – LPB pathway.[51–53] By contrast, PAG, a critical component of the descending pain modulatory system,[20] showed unchanged responses to peripheral stimuli under prolonged activation of dmPFC nociceptive ensemble. Considering a recent study showing that dmPFC – vlPAG maintains pain threshold,[49] we attribute this to rostral-caudal functional difference. In addition, our study does not exclude possible roles of other brain regions evoked by dmPFC nociceptive ensemble activation.

The dmPFC nociceptive ensemble is critical for pain chronicity

Our results show that long-term inhibition of this dmPFC nociceptive ensemble in the early phase relieves the development

Figure 6. Up-regulated neuronal activity and responses to peripheral noxious stimuli of BLA and LPB after prolonged artificial activation of dmPFC nociceptive neurons

(A) Schematic showing AAV2/9-TRE3G-hM3DGq-mCherry or AAV2/9-TRE3G-mCherry injection into the bilateral dmPFC of cfos-htTA mice.

(B) Experimental scheme for virus injection, dox switching, activated neurons label, CNO administration, and behavior test. CNO was administrated (1 mg kg^{-1}, intraperitoneal) during days 1–6 twice per day. Whole-cell current-clamp recording was performed on day 7.

(C) Traces of action potentials (APs) induced by stepped current injection (600 ms, 50 pA step) to dmPFC nociceptive pyramidal neurons after prolonged artificial activation using CNO in mice.

(D) Quantification of APs induced by stepped injected currents to dmPFC nociceptive pyramidal neurons, TRE3G-mCherry group was served as a control (n = 10–11 cells, two-way repeated measure ANOVA with Bonferroni's post hoc test).

(E) Schematic for the activated downstream brain regions screening after long-term artificial activation of dmPFC nociception- or background-labeled neurons.

(F) Confocal images of $shEGFP^+$ cells in BLA, PAG, and LPB after long-term artificial activation of dmPFC nociception or background-labeled neurons. Nuclei in blue (DAPI). Scale bar, 200 μm.

(G) Quantification of $shEGFP^+$ cells across 14 brain regions, normalized by corresponding DAPI number (n = 5 mice, unpaired Student's t test).

(H) Left: Schematic showing fiber implantation into unilateral BLA after AAV2/9-TRE3G-hM3DGq-mCherry injection into bilateral dmPFC and AAV2/9-hSyn-GCaMP6s injection into unilateral BLA of cfos-htTA mice. Right: Time points for fiber photometry recording (upper) and a cartoon mouse receiving laser stimulus on hind paw during fiber photometry recording (lower).

(I) Confocal images of nociceptive neurons in dmPFC and the expression of GCaMP6s in BLA, PAG, and LPB. Scale bar, 200 μm.

(J) Heatmap showing the response of BLA neurons to hind paw laser stimulation on baseline (left), CNO 1 day (middle), and CNO 7 d (right) for nociception-labeling group. Each row represents the response of one trial and white broken line indicates time of the stimulus.

(K) Average fluorescent signals of GCaMP6s expressed in BLA neurons evoked by hind paw laser stimulation on baseline, CNO 1 d, and CNO 7 d in nociception-labeling group (left). Quantification of GCaMP6s fluorescent signals' peak (middle) and area under the curve (AUC) (right) in BLA neurons evoked by paw laser stimulation in nociception-labeling group (n = 4 mice, two trials from each mouse, one-way ANOVA with Bonferroni's post hoc test).

(L) Heatmap showing the response of LPB neurons to hind paw laser stimulation on baseline (left), CNO 1 d (middle), and CNO 7 d (right) for nociception-labeling group. Each row represents the response of one trial and white broken line indicates time of the stimulus.

(M) Average fluorescent signal of GCaMP6s expressed in LPB neurons evoked by hind paw laser stimulation on baseline, CNO 1 d, and CNO 7 d in nociception-labeling group (left). Quantification of GCaMP6s fluorescent peak (middle) and AUC (right) in LPB neurons evoked by paw laser stimulation in nociception-labeling group (n = 3 mice, two trials from each mouse, one-way ANOVA with Bonferroni's post hoc test).

(N) Heatmap showing the response of vlPAG neurons to hind paw laser stimulation on baseline (left), CNO 1 d (middle), and CNO 7 d (right) for nociception-labeling group. Each row represents the response of one trial and white broken line indicates time of the stimulus.

(O) Average fluorescent signals of GCaMP6s expressed in vlPAG neurons evoked by hind paw laser stimulation on baseline, CNO 1 d, and CNO 7 d in nociception-labeling group (left). Quantification of GCaMP6s fluorescent signals' peak (middle) and AUC (right) in vlPAG neurons evoked by paw laser stimulation in nociception-labeling group (n = 3 mice, two trials from each mouse, one-way ANOVA with Bonferroni's post hoc test). *$p < 0.05$, **$p < 0.01$, and ***$p < 0.001$. Data are represented as mean ± SEM, shaded areas indicate SEM. See also Figure S7.

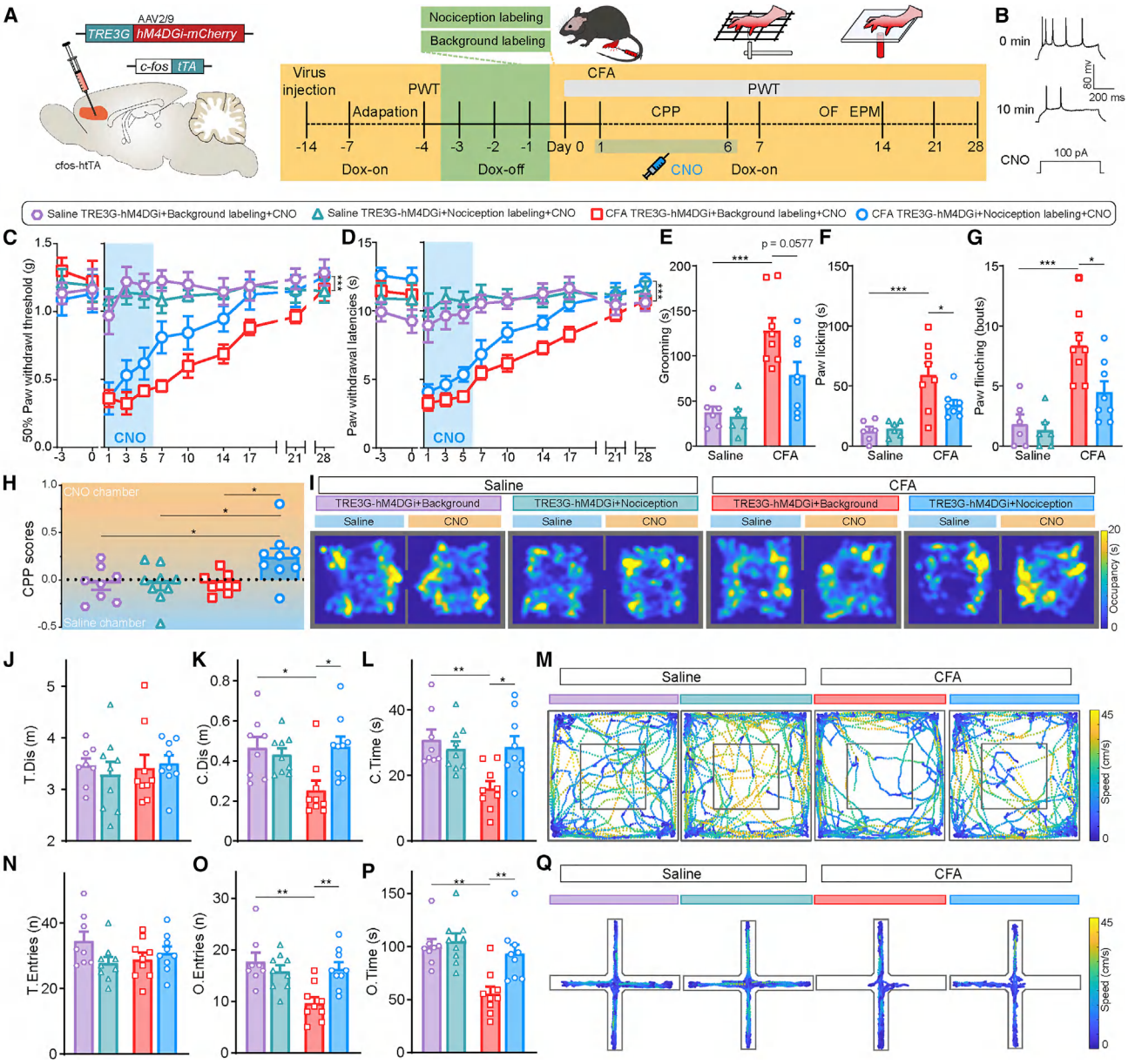

Figure 7. Long-term suppression of dmPFC nociceptive neurons relieves chronic inflammatory pain

(A) Left: Schematic showingAAV2/9-TRE3G-hM4DGi-mCherry injection into the bilateral dmPFC of cfos-htTA mice. Right: Experimental scheme for virus injection, dox switching, activated neurons label, CNO administration, and behavioral test. CNO was administrated (1 mg kg^{-1}, intraperitoneal) during days 1–6 twice per day. Paw withdrawal threshold (PWT) was measured on days −4, 0, 1, 3, 5, 7, 10, 14, 21, and 28. Conditioned place preference (CPP) was measured during days 1–6. Open field (OF) and elevated plus maze (EPM) were measured on day 12 and day 13, respectively.

(B) Whole-cell current-clamp AP recording from hM4DGi expressed dmPFC neurons induced by a depolarizing current (100 pA, 600 ms) before and after bath application of CNO (10 μM, 10 min). The experiment was independently repeated in five neurons from three mice, with similar results obtained.

(C and D) Mechanical paw withdrawal thresholds (C) and thermal paw withdrawal latencies (D) in mice after paw saline or CFA injection (n = 6–9 mice, two-way repeated measure ANOVA with Bonferroni's post hoc test).

(E–G) Time of spontaneous grooming (E), time of spontaneous paw licking (F), and bouts of paw flinching (G) in 20 min on day 3 (n = 6–8 mice, two-way ANOVA with Bonferroni's post hoc test).

(H) CPP score of mice expressing hM4DGi in nociception- or background-labeled neurons after CNO conditioning (n = 8–9 mice, two-way ANOVA with Bonferroni's post hoc test).

(I) Heatmap of the CPP test session, color coded for the relative occupancy time.

(J–L) Quantification of total distance (T.Dis) traveled in the field (J), distance traveled (C.Dis) in the central area (K), and time spent (C.Time) in the central area (L) in the open field test (n = 8–9 mice, two-way ANOVA with Bonferroni's post hoc test).

(M) Exploratory heat traces in the open field, color coded for the movement speed.

(legend continued on next page)

of perceptual hypersensitivity and anxiety in inflammatory pain, consistent with the increased responsive proportion and elevated peak response of this nociceptive ensemble during inflammation pain. On the other side of the coin, prolonged artificial activation of this ensemble elicits chronic pain-like behaviors including mechanical allodynia, thermal hyperalgesia as well as anxiety. We note that anxiety-like symptoms appear much later than allodynia and hyperalgesia, indicating that sensory hypersensitivity precedes the development of anxiety (Figures S5F–S5K). Intriguingly, the thermal hyperalgesia occurs 2 days after CNO administration and rapidly vanishes at the end of CNO treatment. By contrast, the mechanical allodynia occurs later at 4 days after CNO administration, which fades away slowly until 14 days after CNO withdrawal (Figures 5C and 5D). These observations may be explained by different signal processing between mechanical and thermal nociceptive information in brain in the context of pain chronicity.[54] A possible mechanism underlying the perceptual hypersensitivity upon chemogenetic activation is the priming effect, whereas spontaneous pain behaviors and emotional abnormality may arise as a result of long-term neural plasticity alterations. Together, these findings suggest that this dmPFC nociceptive neuronal ensemble is both necessary and sufficient for the development of chronic inflammatory pain.

By sharp contrast, non-specific activation of the entire dmPFC glutamatergic neurons (Figures S6C and S6D) fails to induce chronic pain-like behaviors, which demonstrates the functional heterogeneity among dmPFC neurons. The above observation together with anatomic differences in manipulation might explain the diverse findings of dmPFC's role in CFA-induced inflammatory pain.[17,24] Furthermore, accumulating evidence indicates that subjects with chronic pain experience frequently show enhanced responses following noxious events, reflected in lower pain thresholds and increased pain ratings.[55–59] Similarly, negative treatment experiences have a prolonged effect that can even hamper subsequent unrelated treatment.[60] Finally, patients with central post-stroke pain suffer from intolerable pain on the hemiplegic side although their peripheral sensory inputs are untouched.[61] All this evidence suggests that the recurrence of pain signals alters neural plasticity at both neuronal and circuitry levels. Here we artificially activated dmPFC nociceptive neurons without altering peripheral afferent, and observed enhanced BLA and LPB's neuronal activities and Ca^{2+} signals responding to peripheral nociceptive stimuli, which specifically mimicked the effects of cortical reorganization on recurring nociceptive information only in the brain.

Meanwhile, we need to note that the nociceptive ensemble targeted in the present study may not be the only dmPFC neuronal subpopulation affecting pain chronicity. We applied laser stimuli to achieve genetic labeling of the responsive neurons, which are "evoked" pain engrams in nature. The dmPFC is also involved in mediating spontaneous behaviors, which show distinct brain mechanisms compared with evoked pain.[23,62,63] The spontaneous pain ensemble, if present, could contribute to pain chronicity as well, though possibly through distinct mechanisms. In summary, our study demonstrates that a nociceptive neuronal ensemble in the dmPFC plays an important role in pain chronicity, and indicates the significance to dissect different neuronal subpopulations in elucidating how each brain region modulates pain.

Limitations of the study

Although the cfos-htTA system used in the present study is a classic genetic tool to label activated neuronal ensembles, certain levels of background labeling of non-nociceptive neurons could not be avoided due to the relatively long labeling time window.[64,65] Labeling techniques with higher temporal sensitivity, such as cfos-CreERT2, CANE, and Cal-Light,[66–68] may provide stronger labeling and manipulating specificity. Meanwhile, our proposed model is based on male mice. Previous work has revealed distinct contribution of mPFC in pain modulation between male and female mice with inflammatory pain.[69] Gender as an important biological variable in pain chronicity could be a further direction that could be built from our conclusions and predictions. Another open question that requires further investigation is the dynamic organization of the nociceptive ensemble along the development of chronic pain. While a proportion of dmPFC neurons maintain their nociceptive property at multiple time points after CFA modeling, many others do not show such consistency. Similar phenomena are also revealed by studies on BLA and ACC.[25,70] Whether such dynamic changes of nociceptive neuronal ensembles contribute to certain behavioral dimensions in chronic pain, such as cognitive and affective comorbidity, would be intriguing issues for further investigation.

STAR★METHODS

Detailed methods are provided in the online version of this paper and include the following:

- KEY RESOURCES TABLE
- RESOURCE AVAILABILITY
  - Lead contact
  - Materials availability
  - Data and code availability
- EXPERIMENTAL MODEL AND SUBJECT DETAILS
  - Mouse lines
- METHOD DETAILS
  - Stereotaxic injection
  - Fiber photometry and analysis
  - Miniature two-photon calcium imaging and analysis
  - Nociception labeling
  - Immunostaining
  - Cell counting
  - FACS (fluorescence-activated cell sorting)
  - RNA-seq and analysis

(N–P) Quantification of total arm entries (T.Entries) (N), numbers of entries (O.Entries) into open arms (O), and time spent (O.Time) in open arms (P) in elevated plus maze test (n = 8–9 mice, two-way ANOVA with Bonferroni's post hoc test).
(Q) Exploratory heat traces in the elevated plus maze, color coded for the movement speed. *$p < 0.05$, **$p < 0.01$, and ***$p < 0.001$. Data are represented as mean ± SEM. See also Videos S1 and S2.

- Chemogenetics
- Brain slice electrophysiology
- CFA-induced inflammatory pain
- Behavioral tests

- QUANTIFICATION AND STATISTICAL ANALYSIS

SUPPLEMENTAL INFORMATION

Supplemental information can be found online at https://doi.org/10.1016/j.celrep.2022.111833.

ACKNOWLEDGMENTS

We thank Prof. Haitao Wu for providing us Ai9 transgenic mice and Prof. Yanxue Xue for generously providing cfos-htTA transgenic mice. We also thank Raygene Health Molecular Medicine Technology Co., Ltd. Brain Observatory in the miniature two-photon microscopy and data acquisition for help. This work was funded by grants from the National Natural Science Foundation of China (81974166, 31872774, 32171002), Beijing Natural Science Foundation (7202083), and the National Key R&D Program of China (2017YFA0701302).

AUTHOR CONTRIBUTIONS

X.Q., M.Y., and Y.W. designed experiments and wrote the manuscript; X.Q., K.C., Y.Z., J.T., and W.S. performed the experiments; X.Q., L.W., S.S., L.M., L.X., and K.X. analyzed the data; C.W., X.S., J.W., S.C., and F.L. contributed reagents and discussions; L.M., J.Z., F.L., M.Y., and Y.W. revised the manuscript. M.Y. and Y.W. supervised this study.

DECLARATION OF INTERESTS

The authors declare no competing interests.

Received: March 21, 2022
Revised: July 28, 2022
Accepted: November 22, 2022
Published: December 13, 2022

REFERENCES

1. Global Burden of Disease Study 2013 Collaborators (2015). Global, regional, and national incidence, prevalence, and years lived with disability for 301 acute and chronic diseases and injuries in 188 countries, 1990-2013: a systematic analysis for the global burden of disease study 2013. Lancet *386*, 743–800. https://doi.org/10.1016/S0140-6736(15)60692-4.
2. Williams, A.C.d.C., and Craig, K.D. (2016). Updating the definition of pain. Pain *157*, 2420–2423. https://doi.org/10.1097/j.pain.0000000000000613.
3. Kuner, R., and Kuner, T. (2021). Cellular circuits in the brain and their modulation in acute and chronic pain. Physiol. Rev. *101*, 213–258. https://doi.org/10.1152/physrev.00040.2019.
4. Mercer Lindsay, N., Chen, C., Gilam, G., Mackey, S., and Scherrer, G. (2021). Brain circuits for pain and its treatment. Sci. Transl. Med. *13*, eabj7360. https://doi.org/10.1126/scitranslmed.abj7360.
5. Mansour, A.R., Farmer, M.A., Baliki, M.N., and Apkarian, A.V. (2014). Chronic pain: the role of learning and brain plasticity. Restor. Neurol. Neurosci. *32*, 129–139. https://doi.org/10.3233/RNN-139003.
6. May, A. (2009). New insights into headache: an update on functional and structural imaging findings. Nat. Rev. Neurol. *5*, 199–209. https://doi.org/10.1038/nrneurol.2009.28.
7. Baliki, M.N., Chialvo, D.R., Geha, P.Y., Levy, R.M., Harden, R.N., Parrish, T.B., and Apkarian, A.V. (2006). Chronic pain and the emotional brain: specific brain activity associated with spontaneous fluctuations of intensity of chronic back pain. J. Neurosci. *26*, 12165–12173. https://doi.org/10.1523/JNEUROSCI.3576-06.2006.
8. Kucyi, A., Moayedi, M., Weissman-Fogel, I., Goldberg, M.B., Freeman, B.V., Tenenbaum, H.C., and Davis, K.D. (2014). Enhanced medial prefrontal-default mode network functional connectivity in chronic pain and its association with pain rumination. J. Neurosci. *34*, 3969–3975. https://doi.org/10.1523/JNEUROSCI.5055-13.2014.
9. Metz, A.E., Yau, H.J., Centeno, M.V., Apkarian, A.V., and Martina, M. (2009). Morphological and functional reorganization of rat medial prefrontal cortex in neuropathic pain. Proc. Natl. Acad. Sci. USA *106*, 2423–2428. https://doi.org/10.1073/pnas.0809897106.
10. Wu, X.B., Liang, B., and Gao, Y.J. (2016). The increase of intrinsic excitability of layer V pyramidal cells in the prelimbic medial prefrontal cortex of adult mice after peripheral inflammation. Neurosci. Lett. *611*, 40–45. https://doi.org/10.1016/j.neulet.2015.11.030.
11. Sellmeijer, J., Mathis, V., Hugel, S., Li, X.H., Song, Q., Chen, Q.Y., Barthas, F., Lutz, P.E., Karatas, M., Luthi, A., et al. (2018). Hyperactivity of anterior cingulate cortex areas 24a/24b drives chronic pain-induced anxiodepressive-like consequences. J. Neurosci. *38*, 3102–3115. https://doi.org/10.1523/JNEUROSCI.3195-17.2018.
12. Li, X.Y., Ko, H.G., Chen, T., Descalzi, G., Koga, K., Wang, H., Kim, S.S., Shang, Y., Kwak, C., Park, S.W., et al. (2010). Alleviating neuropathic pain hypersensitivity by inhibiting PKMzeta in the anterior cingulate cortex. Science *330*, 1400–1404. https://doi.org/10.1126/science.1191792.
13. Blom, S.M., Pfister, J.P., Santello, M., Senn, W., and Nevian, T. (2014). Nerve injury-induced neuropathic pain causes disinhibition of the anterior cingulate cortex. J. Neurosci. *34*, 5754–5764. https://doi.org/10.1523/JNEUROSCI.3667-13.2014.
14. Hu, T.T., Wang, R.R., Du, Y., Guo, F., Wu, Y.X., Wang, Y., Wang, S., Li, X.Y., Zhang, S.H., and Chen, Z. (2019). Activation of the intrinsic pain inhibitory circuit from the midcingulate Cg2 to zona incerta alleviates neuropathic pain. J. Neurosci. *39*, 9130–9144. https://doi.org/10.1523/JNEUROSCI.1683-19.2019.
15. Koga, K., Descalzi, G., Chen, T., Ko, H.G., Lu, J., Li, S., Son, J., Kim, T., Kwak, C., Huganir, R.L., et al. (2015). Coexistence of two forms of LTP in ACC provides a synaptic mechanism for the interactions between anxiety and chronic pain. Neuron *85*, 377–389. https://doi.org/10.1016/j.neuron.2014.12.021.
16. Barthas, F., Sellmeijer, J., Hugel, S., Waltisperger, E., Barrot, M., and Yalcin, I. (2015). The anterior cingulate cortex is a critical hub for pain-induced depression. Biol. Psychiatr. *77*, 236–245. https://doi.org/10.1016/j.biopsych.2014.08.004.
17. Wang, G.-Q., Cen, C., Li, C., Cao, S., Wang, N., Zhou, Z., Liu, X.-M., Xu, Y., Tian, N.-X., Zhang, Y., et al. (2015). Deactivation of excitatory neurons in the prelimbic cortex via Cdk5 promotes pain sensation and anxiety. Nat. Commun. *6*, 7660. https://doi.org/10.1038/ncomms8660.
18. Fan, X.C., Fu, S., Liu, F.Y., Cui, S., Yi, M., and Wan, Y. (2018). Hypersensitivity of prelimbic cortex neurons contributes to aggravated nociceptive responses in rats with experience of chronic inflammatory pain. Front. Mol. Neurosci. *11*, 85. https://doi.org/10.3389/fnmol.2018.00085.
19. Cheriyan, J., and Sheets, P.L. (2018). Altered excitability and local connectivity of mPFC-PAG neurons in a mouse model of neuropathic pain. J. Neurosci. *38*, 4829–4839. https://doi.org/10.1523/JNEUROSCI.2731-17.2018.
20. Huang, J., Gadotti, V.M., Chen, L., Souza, I.A., Huang, S., Wang, D., Ramakrishnan, C., Deisseroth, K., Zhang, Z., and Zamponi, G.W. (2019). A neuronal circuit for activating descending modulation of neuropathic pain. Nat. Neurosci. *22*, 1659–1668. https://doi.org/10.1038/s41593-019-0481-5.
21. Jones, A.F., and Sheets, P.L. (2020). Sex-specific disruption of distinct mPFC inhibitory neurons in spared-nerve injury model of neuropathic pain. Cell Rep. *31*, 107729. https://doi.org/10.1016/j.celrep.2020.107729.
22. Zhang, Z., Gadotti, V.M., Chen, L., Souza, I.A., Stemkowski, P.L., and Zamponi, G.W. (2015). Role of prelimbic GABAergic circuits in sensory and emotional aspects of neuropathic pain. Cell Rep. *12*, 752–759. https://doi.org/10.1016/j.celrep.2015.07.001.

23. Ma, L., Yue, L., Zhang, Y., Wang, Y., Han, B., Cui, S., Liu, F.Y., Wan, Y., and Yi, M. (2019). Spontaneous pain disrupts ventral hippocampal CA1-infralimbic cortex connectivity and modulates pain progression in rats with peripheral inflammation. Cell Rep. *29*, 1579–1593.e6. https://doi.org/10.1016/j.celrep.2019.10.002.

24. Dale, J., Zhou, H., Zhang, Q., Martinez, E., Hu, S., Liu, K., Urien, L., Chen, Z., and Wang, J. (2018). Scaling up cortical control inhibits pain. Cell Rep. *23*, 1301–1313. https://doi.org/10.1016/j.celrep.2018.03.139.

25. Corder, G., Ahanonu, B., Grewe, B.F., Wang, D., Schnitzer, M.J., and Scherrer, G. (2019). An amygdalar neural ensemble that encodes the unpleasantness of pain. Science *363*, 276–281. https://doi.org/10.1126/science.aap8586.

26. Cichon, J., Blanck, T.J.J., Gan, W.B., and Yang, G. (2017). Activation of cortical somatostatin interneurons prevents the development of neuropathic pain. Nat. Neurosci. *20*, 1122–1132. https://doi.org/10.1038/nn.4595.

27. Meunier, J.-C., Mollereau, C., Toll, L., Suaudeau, C., Moisand, C., Alvinerie, P., Butour, J.-L., Guillemot, J.-C., Ferrara, P., Monsarrat, B., et al. (1995). Isolation and structure of the endogenous agonist of opioid receptor-like ORL1 receptor. Nature *377*, 532–535. https://doi.org/10.1038/377532a0.

28. Rouillard, A.D., Gundersen, G.W., Fernandez, N.F., Wang, Z., Monteiro, C.D., McDermott, M.G., and Ma'ayan, A. (2016). The harmonizome: a collection of processed datasets gathered to serve and mine knowledge about genes and proteins. Database *2016*, baw100. https://doi.org/10.1093/database/baw100.

29. Deng, J., Zhou, H., Lin, J.K., Shen, Z.X., Chen, W.Z., Wang, L.H., Li, Q., Mu, D., Wei, Y.C., Xu, X.H., and Sun, Y.G. (2020). The parabrachial nucleus directly channels spinal nociceptive signals to the intralaminar thalamic nuclei, but not the amygdala. Neuron *107*, 909–923.e6. https://doi.org/10.1016/j.neuron.2020.06.017.

30. Ewbank, S.N., Campos, C.A., Chen, J.Y., Bowen, A.J., Padilla, S.L., Dempsey, J.L., Cui, J.Y., and Palmiter, R.D. (2020). Chronic Gq signaling in AgRP neurons does not cause obesity. Proc. Natl. Acad. Sci. USA *117*, 20874–20880. https://doi.org/10.1073/pnas.2004941117.

31. Pati, S., Saba, K., Salvi, S.S., Tiwari, P., Chaudhari, P.R., Verma, V., Mukhopadhyay, S., Kapri, D., Suryavanshi, S., Clement, J.P., et al. (2020). Chronic postnatal chemogenetic activation of forebrain excitatory neurons evokes persistent changes in mood behavior. Elife *9*, e56171. https://doi.org/10.7554/eLife.56171.

32. Apkarian, A.V., Sosa, Y., Sonty, S., Levy, R.M., Harden, R.N., Parrish, T.B., and Gitelman, D.R. (2004). Chronic back pain is associated with decreased prefrontal and thalamic gray matter density. J. Neurosci. *24*, 10410–10415. https://doi.org/10.1523/JNEUROSCI.2541-04.2004.

33. Tajerian, M., Leu, D., Zou, Y., Sahbaie, P., Li, W., Khan, H., Hsu, V., Kingery, W., Huang, T.T., Becerra, L., and Clark, J.D. (2014). Brain neuroplastic changes accompany anxiety and memory deficits in a model of complex regional pain syndrome. Anesthesiology *121*, 852–865. https://doi.org/10.1097/ALN.0000000000000403.

34. Bliss, T.V.P., Collingridge, G.L., Kaang, B.K., and Zhuo, M. (2016). Synaptic plasticity in the anterior cingulate cortex in acute and chronic pain. Nat. Rev. Neurosci. *17*, 485–496. https://doi.org/10.1038/nrn.2016.68.

35. Calo, G., Guerrini, R., Rizzi, A., Salvadori, S., and Regoli, D. (2000). Pharmacology of nociceptin and its receptor: a novel therapeutic target. Br. J. Pharmacol. *129*, 1261–1283. https://doi.org/10.1038/sj.bjp.0703219.

36. Ferrer, I., Garcia-Esparcia, P., Carmona, M., Carro, E., Aronica, E., Kovacs, G.G., Grison, A., and Gustincich, S. (2016). Olfactory receptors in non-chemosensory organs: the nervous system in Health and disease. Front. Aging Neurosci. *8*, 163. https://doi.org/10.3389/fnagi.2016.00163.

37. Gaudel, F., Guiraudie-Capraz, G., and Féron, F. (2021). Limbic expression of mRNA coding for chemoreceptors in human brain-lessons from brain atlases. Int. J. Mol. Sci. *22*, 6858. https://doi.org/10.3390/ijms22136858.

38. Liang, B., Zhang, L., Barbera, G., Fang, W., Zhang, J., Chen, X., Chen, R., Li, Y., and Lin, D.T. (2018). Distinct and dynamic on and off neural ensembles in the prefrontal cortex code social exploration. Neuron *100*, 700–714.e9. https://doi.org/10.1016/j.neuron.2018.08.043.

39. Ye, L., Allen, W.E., Thompson, K.R., Tian, Q., Hsueh, B., Ramakrishnan, C., Wang, A.C., Jennings, J.H., Adhikari, A., Halpern, C.H., et al. (2016). Wiring and molecular features of prefrontal ensembles representing distinct experiences. Cell *165*, 1776–1788. https://doi.org/10.1016/j.cell.2016.05.010.

40. Zhang, C., Zhu, H., Ni, Z., Xin, Q., Zhou, T., Wu, R., Gao, G., Gao, Z., Ma, H., Li, H., et al. (2022). Dynamics of a disinhibitory prefrontal microcircuit in controlling social competition. Neuron *110*, 516–531.e6. https://doi.org/10.1016/j.neuron.2021.10.034.

41. Kim, J., Pignatelli, M., Xu, S., Itohara, S., and Tonegawa, S. (2016). Antagonistic negative and positive neurons of the basolateral amygdala. Nat. Neurosci. *19*, 1636–1646. https://doi.org/10.1038/nn.4414.

42. Sørensen, A.T., Cooper, Y.A., Baratta, M.V., Weng, F.J., Zhang, Y., Ramamoorthi, K., Fropf, R., LaVerriere, E., Xue, J., Young, A., et al. (2016). A robust activity marking system for exploring active neuronal ensembles. Elife *5*, e13918. https://doi.org/10.7554/eLife.13918.

43. Carrillo-Reid, L., Yang, W., Bando, Y., Peterka, D.S., and Yuste, R. (2016). Imprinting and recalling cortical ensembles. Science *353*, 691–694. https://doi.org/10.1126/science.aaf7560.

44. Pozhidayeva, D.Y., Farris, S.P., Goeke, C.M., Firsick, E.J., Townsley, K.G., Guizzetti, M., and Ozburn, A.R. (2020). Chronic chemogenetic stimulation of the nucleus accumbens produces lasting reductions in binge drinking and ameliorates alcohol-related morphological and transcriptional changes. Brain Sci. *10*, 109.

45. Gabbott, P.L.A., Warner, T.A., Jays, P.R.L., Salway, P., and Busby, S.J. (2005). Prefrontal cortex in the rat: projections to subcortical autonomic, motor, and limbic centers. J. Comp. Neurol. *492*, 145–177. https://doi.org/10.1002/cne.20738.

46. George, O., and Koob, G.F. (2010). Individual differences in prefrontal cortex function and the transition from drug use to drug dependence. Neurosci. Biobehav. Rev. *35*, 232–247. https://doi.org/10.1016/j.neubiorev.2010.05.002.

47. Croxson, P.L., Johansen-Berg, H., Behrens, T.E.J., Robson, M.D., Pinsk, M.A., Gross, C.G., Richter, W., Richter, M.C., Kastner, S., and Rushworth, M.F.S. (2005). Quantitative investigation of connections of the prefrontal cortex in the human and macaque using probabilistic diffusion tractography. J. Neurosci. *25*, 8854–8866. https://doi.org/10.1523/JNEUROSCI.1311-05.2005.

48. Smith, M.L., Asada, N., and Malenka, R.C. (2021). Anterior cingulate inputs to nucleus accumbens control the social transfer of pain and analgesia. Science *371*, 153–159. https://doi.org/10.1126/science.abe3040.

49. Yin, J.B., Liang, S.H., Li, F., Zhao, W.J., Bai, Y., Sun, Y., Wu, Z.Y., Ding, T., Sun, Y., Liu, H.X., et al. (2020). dmPFC-vlPAG projection neurons contribute to pain maintenance thresholds and anxiolytic behaviors. J. Clin. Invest. https://doi.org/10.1172/JCI127607.

50. Sun, L., Liu, R., Guo, F., Wen, M.Q., Ma, X.L., Li, K.Y., Sun, H., Xu, C.L., Li, Y.Y., Wu, M.Y., et al. (2020). Parabrachial nucleus circuit governs neuropathic pain-like behavior. Nat. Commun. *11*, 5974. https://doi.org/10.1038/s41467-020-19767-w.

51. Raver, C., Uddin, O., Ji, Y., Li, Y., Cramer, N., Jenne, C., Morales, M., Masri, R., and Keller, A. (2020). An amygdalo-parabrachial pathway regulates pain perception and chronic pain. J. Neurosci. *40*, 3424–3442. https://doi.org/10.1523/JNEUROSCI.0075-20.2020.

52. Song, J., Shao, D., Guo, X., Zhao, Y., Cui, D., Ma, Q., Sheng, H., Ma, L., Lai, B., Chen, M., and Zheng, P. (2019). Crucial role of feedback signals from prelimbic cortex to basolateral amygdala in the retrieval of morphine withdrawal memory. Sci. Adv. *5*, eaat3210. https://doi.org/10.1126/sciadv.aat3210.

53. Janak, P.H., and Tye, K.M. (2015). From circuits to behaviour in the amygdala. Nature *517*, 284–292. https://doi.org/10.1038/nature14188.

54. Cai, Y.Q., Wang, W., Paulucci-Holthauzen, A., and Pan, Z.Z. (2018). Brain circuits mediating opposing effects on emotion and pain. J. Neurosci. *38*, 6340–6349. https://doi.org/10.1523/JNEUROSCI.2780-17.2018.

55. Bachiocco, V., Scesi, M., Morselli, A.M., and Carli, G. (1993). Individual pain history and familial pain tolerance models: relationships to post-surgical pain. Clin. J. Pain *9*, 266–271. https://doi.org/10.1097/00002508-199312000-00008.

56. Lidow, M.S. (2002). Long-term effects of neonatal pain on nociceptive systems. Pain *99*, 377–383. https://doi.org/10.1016/s0304-3959(02)00258-0.

57. Ren, K., Anseloni, V., Zou, S.P., Wade, B.E., Novikova, I.S., Ennis, M., Traub, J.R., Gold, S.M., Dubner, R., and Lidow, S.M. (2004). Characterization of basal and re-inflammation-associated long-term alteration in pain responsivity following short-lasting neonatal local inflammatory insult. Pain *110*, 588–596. https://doi.org/10.1016/j.pain.2004.04.006.

58. Hermann, C., Hohmeister, J., Demirakça, S., Zohsel, K., and Flor, H. (2006). Long-term alteration of pain sensitivity in school-aged children with early pain experiences. Pain *125*, 278–285. https://doi.org/10.1016/j.pain.2006.08.026.

59. Wegner, A., Elsenbruch, S., Rebernik, L., Roderigo, T., Engelbrecht, E., Jäger, M., Engler, H., Schedlowski, M., and Benson, S. (2015). Inflammation-induced pain sensitization in men and women: does sex matter in experimental endotoxemia? Pain *156*, 1954–1964. https://doi.org/10.1097/j.pain.0000000000000256.

60. Kessner, S., Forkmann, K., Ritter, C., Wiech, K., Ploner, M., and Bingel, U. (2014). The effect of treatment history on therapeutic outcome: psychological and neurobiological underpinnings. PLoS One *9*, e109014. https://doi.org/10.1371/journal.pone.0109014.

61. Klit, H., Finnerup, N.B., and Jensen, T.S. (2009). Central post-stroke pain: clinical characteristics, pathophysiology, and management. Lancet Neurol. *8*, 857–868. https://doi.org/10.1016/S1474-4422(09)70176-0.

62. Ong, W.Y., Stohler, C.S., and Herr, D.R. (2019). Role of the prefrontal cortex in pain processing. Mol. Neurobiol. *56*, 1137–1166. https://doi.org/10.1007/s12035-018-1130-9.

63. Khan, S.A., Keaser, M.L., Meiller, T.F., and Seminowicz, D.A. (2014). Altered structure and function in the hippocampus and medial prefrontal cortex in patients with burning mouth syndrome. Pain *155*, 1472–1480. https://doi.org/10.1016/j.pain.2014.04.022.

64. Liu, X., Ramirez, S., Pang, P.T., Puryear, C.B., Govindarajan, A., Deisseroth, K., and Tonegawa, S. (2012). Optogenetic stimulation of a hippocampal engram activates fear memory recall. Nature *484*, 381–385. https://doi.org/10.1038/nature11028.

65. Reijmers, L.G., Perkins, B.L., Matsuo, N., and Mayford, M. (2007). Localization of a stable neural correlate of associative memory. Science *317*, 1230–1233. https://doi.org/10.1126/science.1143839.

66. Guenthner, C.J., Miyamichi, K., Yang, H.H., Heller, H.C., and Luo, L. (2013). Permanent genetic access to transiently active neurons via TRAP: targeted recombination in active populations. Neuron *78*, 773–784. https://doi.org/10.1016/j.neuron.2013.03.025.

67. Lee, D., Hyun, J.H., Jung, K., Hannan, P., and Kwon, H.B. (2017). A calcium- and light-gated switch to induce gene expression in activated neurons. Nat. Biotechnol. *35*, 858–863. https://doi.org/10.1038/nbt.3902.

68. Sakurai, K., Zhao, S., Takatoh, J., Rodriguez, E., Lu, J., Leavitt, A.D., Fu, M., Han, B.X., and Wang, F. (2016). Capturing and manipulating activated neuronal ensembles with CANE delineates a hypothalamic social-fear circuit. Neuron *92*, 739–753. https://doi.org/10.1016/j.neuron.2016.10.015.

69. Cardenas, A., Papadogiannis, A., and Dimitrov, E. (2021). The role of medial prefrontal cortex projections to locus ceruleus in mediating the sex differences in behavior in mice with inflammatory pain. Faseb. J. *35*, e21747. https://doi.org/10.1096/fj.202100319RR.

70. Acuña, M.A., Kasanetz, F., De Luna, P., and Nevian, T. (2020). Cortical representation of pain by stable dedicated neurons and dynamic ensembles. Preprint at bioRxiv. https://doi.org/10.1101/2020.11.02.364778.

71. MacArthur Clark, J.A., and Sun, D. (2020). Guidelines for the ethical review of laboratory animal welfare people's Republic of China national standard GB/T 35892-2018 [issued 6 february 2018 effective from 1 september 2018]. Animal Model. Exp. Med. *3*, 103–113. https://doi.org/10.1002/ame2.12111.

72. Pachitariu, M., Stringer, C., Dipoppa, M., Schröder, S., Rossi, L.F., Dalgleish, H., Carandini, M., and Harris, K.D. (2017). Suite2p: beyond 10,000 neurons with standard two-photon microscopy. Preprint at bioRxiv, 061507. https://doi.org/10.1101/061507.

73. Keith, B.J., Franklin, M., and Paxinos, G. (2008). The Mouse Brain in Stereotaxic Coordinates, Compact: The Coronal Plates and Diagrams (Elsevier Science).

74. Raudvere, U., Kolberg, L., Kuzmin, I., Arak, T., Adler, P., Peterson, H., and Vilo, J. (2019). g:Profiler: a web server for functional enrichment analysis and conversions of gene lists (2019 update). Nucleic Acids Res. *47*, W191–W198. https://doi.org/10.1093/nar/gkz369.

75. Jiang, Y.Y., Shao, S., Zhang, Y., Zheng, J., Chen, X., Cui, S., Liu, F.Y., Wan, Y., and Yi, M. (2018). Neural pathways in medial septal cholinergic modulation of chronic pain: distinct contribution of the anterior cingulate cortex and ventral hippocampus. Pain *159*, 1550–1561. https://doi.org/10.1097/j.pain.0000000000001240.

76. Dixon, W.J., and Mood, A.M. (1948). A method for obtaining and analyzing sensitivity data. J. Am. Stat. Assoc. *43*, 109–126. https://doi.org/10.1080/01621459.1948.10483254.

STAR★METHODS

KEY RESOURCES TABLE

REAGENT or RESOURCE	SOURCE	IDENTIFIER
Antibodies		
Mouse Anti-VgluT2	Abcam	CAT # ab79157; RRID: AB_1603114
Rabbit Anti-GAD65&67	Abcam	CAT # ab183999
Goat anti-mouse IgG-Alexa 594	ZSGB-BIO	CAT # ZF-0516
Goat anti-rabbit IgG-Alexa 647	Abcam	CAT # ab150079; RRID: AB_2722623
Bacterial and virus strains		
AAV2/9-hSyn-GCaMP6s	BrainVTA	N/A
AAV2/9-TRE3G-mCherry	Vigene Technology	N/A
AAV2/9-TRE3G-hM3DGq-mCherry	Vigene Technology	N/A
AAV2/9-TRE3G-hM4DGi-mCherry	BrainVTA	N/A
AAV2/9-CaMKII-hM3DGq-mCherry	BrainVTA	N/A
AAV2/1-hSyn-Cre	BrainVTA	N/A
AAV2/Retro-hSyn-mCherry	BrainVTA	N/A
Chemicals, peptides, and recombinant proteins		
Clozapine-*N*-oxide	Tocris	CAT # 4936/50
Complete Freund's adjuvant	Sigma-Aldrich	CAT # F5881-10ML
DAPI	Cell Signaling Technology	CAT # 4083S
Papain	Worthington	CAT # LS003119
Deposited data		
Nociception & Background labeling neuron transcriptome sequencing	This study	NCBI_bioproject: PRJNA825413 https://www.ncbi.nlm.nih.gov/bioproject/PRJNA825413
Experimental models: Organisms/strains		
Mouse: C57BL/6N	Department of Laboratory Animal Sciences, Peking University Health Science Center	JAX 000664; RRID: IMSR_JAX:000664
Mouse: cfos-htTA	The Jackson Laboratory	JAX 018306; RRID: IMSR_JAX:018306
Mouse: Ai9	The Jackson Laboratory	JAX 007905; RRID: IMSR_JAX:007905
Software and algorithms		
Fiji (ImageJ)	NIH	https://fiji.sc/
GraphPad Prism 9	GraphPad	https://www.graphpad.com/scientificsoftware/prism/
Origin 2022b	OriginLab	https://www.originlab.com/
MATLAB	MathWorks	https://www.mathworks.com
Smart	Panlab	https://www.panlab.com/en/products/smart-video-tracking-software-panlab
Suite2p	HHMI Janelia Research Campus	https://www.suite2p.org/

RESOURCE AVAILABILITY

Lead contact

Further information and requests for resources and reagents should be directed to and will be fulfilled by the lead contact, Ming Yi (mingyi@hsc.pku.edu.cn).

Materials availability

This study did not generate new unique reagents.

Data and code availability

- The accession number for the transcriptome sequencing reported in this paper is Sequence Read Archive (SRA): SUB11224161.
- This paper does not report original code.
- Any additional information required to reanalyze the data reported in this work paper is available from the lead contact upon request.

EXPERIMENTAL MODEL AND SUBJECT DETAILS

Mouse lines

Male C57BL/6N, cfos-htTA, Ai9 mice at the age of 6–12 weeks old were used for experiments. C57BL/6N mice were purchased from Department of Laboratory Animal Sciences, Peking University Health Science Center. Ai9 mice were acquired from Prof. Haitao Wu (Institute of Basic Medical Sciences, Beijing, China), cfos-htTA mice were acquired from Prof. Yanxue Xue (National Institute on Drug Dependence, Peking University, Beijing, China). All mice were housed under pathogen-free circumstances, with a 12 h artificially alternating light/dark cycle and ad libitum feeding. All behavioral testing were performed in dark cycle of mice. The cfos-htTA mice were fed with food containing 40 mg kg^{-1} Dox for 1 week before surgery. All animal experiments followed the guidelines of the Committee for Research and Ethical Issues of the International Association for the Study of Pain and were approved by the Animal Care and Use Committee of Peking University Health Science Center.[71]

METHOD DETAILS

Stereotaxic injection

For intracranial virus injection, mice were anesthetized with 1% sodium pentobarbitone (100 mg kg^{-1}) intraperitoneally (*i.p.*) and mounted in a stereotaxic frame (RWD, China). Body temperature of mice was maintained with a heating pad (RWD, China). Ophthalmic ointment was applied to eyes before the skull was exposed by midline scalp incision, then a small craniotomy was performed using a handheld drill (RWD, China) over target site. Viruses were injected into target brain areas using an oil pressure system [glass pipette was filled with mineral oil and connected to a microsyringe which was controlled by a syringe pump (kd Scientific, USA), virus was filled into the pipette without air bubble]. A total of 0.3 μL of AAV was injected into unilateral dmPFC [anteroposterior (AP) from bregma: +1.65 mm; mediolateral (ML) from midline: ±0.3 mm; dorsoventral (DV) from dura: −1.65 mm], AcbC (AP: +1.6 mm; ML: ±1.2 mm; DV: −3..55 mm), BLA (AP: −1.6 mm; ML: ±2.8 mm; DV: −3.8 mm), PAG (AP: 4.2 mm; ML: ±0.3 mm; DV: −2.7 mm), or LPB (AP: −5.1 mm; ML: ±1.3 mm; DV: −2.3 mm) at a flow rate of 60 nL/min. After injection, needles were left in place for an additional 5 min before it was slowly withdrawn to minimize spread of viral particles along the injection tract. Then, skin was sutured and mice were put on a heating blanket before returning to their home cages. Mice were given 4–6 weeks for recovery from surgery and virus expression. Injection sites were verified histologically after behavioral testing. Subjects with off-target expression were excluded from further analysis.

Fiber photometry and analysis

Mice were disposed through similar procedures as stereotaxic injection described above. After AAV2/9-hSyn-GCaMP6s virus injection into dmPFC, BLA, PAG and LPB, 0.2 mm diameter optic fiber cannulas (NA = 0.37, INPER, China) were implanted into dmPFC until the tip was placed −0.2 mm above virus injection target and secured in place with denture base resins (Medental, China). Mice were given 4–6 weeks for recovery from surgery and virus expression. GCaMP6s signals were recorded using a Fiber Photometry system (INPER, China), with the 480 nm LED power of 40 μW and the 410 nm LED power of 30 μW.

Mouse was allowed to move freely in a transparent plastic chamber (10 cm × 10 cm × 15 cm) with video recording. Each mouse was handled and adapted in chamber for 10 min per day in 3 consecutive days before the first time of recording. Floor of the chamber was a grid plate with stainless steel bars of 2 mm in diameter and 5 mm in between. Recording was performed when mice were quietly awake. To test dmPFC neuronal activity in response to mechanical stimulation, mice received prick using the pin (37 mm long and 0.56 mm in diameter) onto the hind paw, or light mechanical stimuli onto the hind paw using a brush. To examine neural activity of dmPFC, BLA, PAG and LPB in response to thermal stimulation, mice received laser stimuli onto the hind paw using an ultra-pulse carbon dioxide laser therapeutic machine (DM-300, DIMEI, China) with 4–6 W power and 5 ms emission duration. For testing the dmPFC neuronal activity in response to aversive stimulation, mice received air puff on the face using a rubber suction bulb.

Data were analyzed using MATLAB. For dmPFC recording, values of Ca^{2+} transients change (ΔF/F) from −5 s to 20 s (0 s, stimuli onset) were derived by calculating $(F - F_0)/F_0$ for each trial, where F_0 was defined as the mean Ca^{2+} transients from −5 s to 0 s. For recording of BLA, PAG and LPB, ΔF/F from −2 s to 10 s (0 s, stimuli onset) were derived as above, where F_0 was defined as the mean Ca^{2+} transients from −2 s to 0 s. Values of peak and AUC (area under cure) were normalized by corresponding mean value of Pre-CNO. Subjects with off-target fiber ends location were excluded from analysis.

Miniature two-photon calcium imaging and analysis

Mice were disposed through similar procedures as stereotaxic injection described above. After AAV2/9-hSyn-GCaMP6s virus injection into dmPFC, a 0.6 mm diameter, ~4 mm length gradient refractive index lens (GRIN lens; GoFoton, USA) was slowly advanced into dmPFC until the tip was placed at DV: −1.5 mm. After 3–4 weeks of viral expression, an imaging baseplate was positioned over the GRIN lens and cemented with denture base resins. The miniature two-photon microscope (FHIRMTPM V2.0, field of view: 420 × 420 mm^2; resolution: ~1.13 μm; working distance: 1 mm) was detachable while its holder was mounted permanently onto a baseplate over the GRIN lens. Cover of the holder and protective glue (Kwik-Cast, WPI Inc, USA) on the GRIN lens were removed before imaging. Then headpiece was mounted on the holder and locked with M2 screws. Imaging data was acquired using imaging software (GINKGO-MTPM, Transcend Vivoscope Biotech Co., Ltd, China) at a frame rate of 10 Hz (512 × 512 pixels) with a 920 nm femtosecond fiber laser (~35 mW at the objective, TVS-FL-01, Transcend Vivoscope Biotech Co.Ltd, China). Timestamps of imaging frames were marked according to the controller (TVS-MMM-01, Transcend Vivoscope Biotech Co., Ltd, China).

Mouse was allowed to move freely in a transparent plastic chamber (10 cm × 10 cm × 15 cm) with video recording. Each mouse was handled and adapted in chamber for 10 min per day in 3 consecutive days, before the first time of recording. Floor of the chamber was a grid plate with stainless steel bars of 2 mm in diameter and 5 mm in between. Recording (10 frames per sec) was performed when mice were quietly awake on days 0, 1, 3 and 9 after hind paw CFA injection. Three stimuli (noxious pin prick, noxious laser and mild touch by 0.4 g *von Frey* fiber) were performed 10 times with 30 s intervals.

Motion correction, registration, cell detection and signal extraction were performed *via* Suite2p[72] followed by manually correction. Cell signal was converted to relative changes in fluorescence (dff) using the following formula: $dff = \Delta F/F_0 = (F - F_0)/F_0$, where F_0 was the mean signal over the entire movie in every recording day. To determine which neuron significantly responded to each stimulus, the fluorescent signal was extracted at the period that −5 s ~ −3 s before and 0 s–5 s after stimulus onset. One-tailed Wilcoxon rank-sum test was performed for responsive neuron identification. We designated any neurons for which $p < 0.05$ as being significantly responsive to stimulus. To assess whether the spontaneous firing rate of dmPFC neurons changed, recording of spontaneous firing events was performed 5 min before delivering stimuli. After transforming the signal to dff and spatially smoothing it by averaging over a 600 ms sliding window, we took the time-derivative of the resulting trace, calculated the standard deviation (s.d.) for each signal, and identified any peaks that were >2 s.d. as spontaneous transient events while enforcing a limit of a minimum inter-event time of >20 frames (2 s).

Nociception labeling

Laser stimulation was generated by an ultra-pulse carbon dioxide laser therapeutic machine (DM-300, DIMEI, China) and delivered to hind paw of mice from the guide arm. Tip of the guide arm was kept away from the plantar surface of the hind paw at a distance of 2 cm. Focus of laser beam was altered a little bit from trial to trial to avoid possible tissue damage. Laser power ranged from 4 to 6 W with an emission time of 5 ms. The power used for each mouse was the lowest power to induce >3 trials with paw lifting behavior in 5 laser stimuli, determined by a pilot experiment.

For activated brain region screening, each mouse was handled for 5 min and adapted in a plexiglas cube for 30 min per day in 3 consecutive days before nociception labeling. On stimulation day, each mouse received laser stimulation (4–6 W, 5 ms) alternatively onto left or right hind paw every 5 min for 2 h. After that, mice were perfused immediately for following activated brain region screening.

For nociception activated neurons labeling, two weeks after recovery from virus injection surgery, each mouse was handled for 5 min and adapted in a plexiglas cube for 30 min per day in 3 consecutive days while fed on 40 mg kg^{-1} Dox food. Following the third adaptation, mice were fed with regular food without Dox for 2 days. On stimulation day, mice received three stimulation sessions separated by 4 h in their home cages. For each stimulation session, each mouse received laser stimulation (4–6 W, 5 ms) alternatively onto left or right hind paw every 5 min for 1 h. After the third stimulation session, mice were returned to its home cage and fed with food containing 1 g kg^{-1} Dox overnight to rapidly turn off any additional virus expression. Then mice had been kept with 40 mg kg^{-1} Dox food till the end of experiment.

For background activated neurons labeling, the mice were treated in the same manner as the nociception activated neurons labeling group except for stimulation session, where mice were placed in the same plexiglas cube for 1 h without receiving laser stimulation onto hind paws.

Immunostaining

Mice were anesthetized with 1% pentobarbital sodium (100 mg kg^{-1}, *i.p.*) and intracardially perfused with normal saline followed by 4% paraformaldehyde (PFA) in 0.01 M phosphate buffer (PB, pH 7.4). Brains were postfixed with 4% PFA for 12 h, and dehydrated using 20% and 30% sucrose solutions in turn. After embedded in optimal cutting temperature compound, brains were sectioned coronally into 50-μm slices on a freezing microtome (Model 3050s, Leica, Germany). Free-floating sections were washed in phosphate-buffered saline (PBS) for three times, and then incubated with PBST-BSA (0.3% Triton X-100 and 5% bull serum albumin in PBS) for 30 min at room temperature. After those sections were incubated with primary antibodies at 4°C overnight (1:200 dilution in 0.3% PBST for all primary antibodies). Then sections washed 5 × 5 min with PBST, and incubated with secondary antibodies at room temperature for 90 min (1:500 dilution in 0.3% PBST for all secondary antibodies). After 5 × 5 min washing with PBST again,

sections were finally mounted with a sealing buffer (pH 9.0) containing $NaHCO_3$ (220.2 mM), Na_2CO_3 (28.3 mM), 50% glycerol and 4′,6-diamidino-2-phenylindole (DAPI, 1:10,000). Images were taken by a laser-scanning confocal microscope (model FV1000, Olympus, Japan).

Cell counting

For activated brain region screening, the brain slices of cfos-htTA mice did not require immunohistochemistry to visualize neurons with nuclear localized shEGFP, therefore sections containing brain regions of interest were mounted with sealing buffer and DAPI (1:10,000) immediately after slicing. Brain regions were defined using the Mouse Brain Atlas parameters,[73] all $shEGFP^+$ cells and DAPI stained nuclei within designated brain regions were counted automatically using Fiji. The level of activation in different brain regions was normalized by calculating ($shEGFP^+$ neurons)/DAPI.

For VGlut2 and GAD65&67 staining, the number of $shEGFP^+$ cells within the designated brain regions were counted automatically while VGlut2/GAD65&67 and shEGFP double-positive cells were counted manually using Fiji. Percentage of excitatory and inhibitory neuron in nociception was calculated as ($VGlut2^+$ and $shEGFP^+$ cells)/($shEGFP^+$ cells) and ($GAD65\&67^+$ and $shEGFP^+$ cells)/($shEGFP^+$ cells) respectively.

For labeling and reactivation efficiency test of Tet-off system, sections containing dmPFC were mounted as above immediately after labeling or nociception restimulating. The number of $mCherry^+$ cells and DAPI stained nuclei within designated brain regions were counted automatically while $mCherry^+$ and $shEGFP^+$ cells were counted manually using Fiji. The amount of reactivation was normalized for chance level, whose formula is defined as follows:

All images were taken by a laser-scanning confocal microscope (model FV1000, Olympus, Japan), and cell counting was conducted by a researcher blind to experimental condition. Averages for each study were determined from across three to four slices from four to six mice in each group.

FACS (fluorescence-activated cell sorting)

Mice were executed by cervical dislocation and brains were acutely removed. The dmPFC were isolated on ice with a mouse brain matrice, mechanically dissociated in DMEM/F12 media, and then incubated with papain (1 mg mL^{-1}) for 30 min at 37°C. Then tissue pieces were dissociated into single cells by gentle trituration and filtered through a 70 μm cell strainer (F613462, BBI). Sorting was performed using a fluorescence-activated cell sorter (BD Biosciences) in the single-cell sorting mode selecting cells with high mCherry fluorescence. Cells were collected in tubes with lysis component and ribonuclease inhibitor for subsequent RNA sequencing.

RNA-seq and analysis

The amplification was carried out by the Smart-Seq2 method. An Oligo dT primer was introduced to the reverse transcription reaction for first strand cDNA synthesis, followed by PCR amplification to enrich cDNA and magnetic beads purification to clean up the production. Then, the cDNA production was examinedby Qubit 3.0 Fluorometer (Thermo Fisher Scientific, USA) and Agilent 2100 Bioanalyzer (Agilent, USA) to ensure the expected production with length around 1–2 kbp. Then, the cDNA was sheared randomly by ultrasonic waves for Illumina library preparation protocol including DNA fragmentation, end repair, 3′ ends A-tailing, adapter ligation, PCR amplification and library validation. After library preparation, PerkinElmer LabChip GX Touch and Step OnePlus Real-Time PCR System were introduced for library quality inspection. Qualified libraries were then loaded on illumina Hiseq platform (illumina, USA) for PE150 sequencing.

The Clean Data were filtered, which were statistically for the quality and data quantity, including Q30 statistics, data quantity statistics, base content statistics, *etc*. Reference gene and genome annotation files downloaded from the UCSC (http://hgdownload.soe.ucsc.edu/goldenPath/galGal4), using Bowtie2 to build the reference genome library, and then the clean data were mapped to the reference genome by TopHat. HTSeq was run to calculate counts of each gene, and RPKM (Reads Per Kilobase of exon model per Million mapped reads) was used to asses expression quantity.

Differentially expressed genes were detected by DESeq2 with library batches as covariate. Genes were considered to be differentially expressed if the Benjamin–Hochberg adjusted p value was below 0.05 and the fold change was above 2. Gene Ontology (GO) annotation enrichment analysis were conducted by g:Profiler[74] with the Benjamin–Hochberg adjusted $p < 0.05$ is considered as statistically significant.

Chemogenetics

Clozapine *N*-oxide (CNO; Tocris, UK) was initially dissolved in DMSO to stock concentration (20 mg mL^{-1}), then diluted to working concentration in normal saline (0.2 mg mL^{-1}). For chemogenetic manipulation of dmPFC labeled neurons, mice were injected with CNO (1 mg kg^{-1}, *i.p.*) 30 min before behavioral assessment. Same amounts of saline with 1% DMSO were injected as controls. The dosage of CNO was selected on the basis of both published studies[75] and our pilot experiments.

Brain slice electrophysiology

Mice were executed by cervical dislocation and brains were rapidly dissected and submerged in ice-cold, oxygenated (95% O_2, 5% CO_2) cutting solution containing KCl (2.5 mM), NaH_2PO_4 (1.25 mM), $CaCl_2$ (0.5 mM), $MgSO_4$ (10 mM), $NaHCO_3$ (26 mM), glucose (10 mM), and sucrose (230 mM), pH 7.4, 300–310 mOsm. Coronal slices (250 μm) containing dmPFC were cut with a Leica

VT1000S vibrating microtome (Leica Instruments, Germany) and transferred to an incubation chamber with oxygenated, warm (32°C) regular artificial cerebrospinal fluid (ACSF) containing NaCl (126 mM), KCl (2.5 mM), $MgCl_2$ (1.3 mM), NaH_2PO_4 (1.2 mM), $CaCl_2$ (2.4 mM), $NaHCO_3$ (18 mM), and glucose (10 mM), pH 7.4, 290–300 mOsm. Slices were then allowed to equilibrate for ~1 h at room temperature.

After the recovery period, individual slices were placed in a submerged recording chamber, and the tissue was continuously perfused (2 mL min^{-1}) with ACSF. The recording chamber was placed on the fixed stage of an Olympus BX51 microscope (Olympus, Japan) equipped with video-enhanced infrared differential interference contrast. Whole-cell recordings were obtained from fluorescence positive neurons of dmPFC. Patch pipettes were pulled from borosilicate glass capillary tubes (Sutter, USA) using a PC-10 pipette puller (Narishige, Japan). Resistance of pipettes varied between 5 and 8 MΩ when filled with a K^+-Met-sulfonate intracellular solution containing K^+-Met-sulfonate (140.5 mM), NaCl (7.5 mM), 4-(2-hydroxyethyl)-1-piperazineethanesulfonic acid (HEPES) hemisodium salt (10 mM), Mg-ATP (2 mM), and Na-GTP (0.2 mM), pH 7.33, 300–310 mOsm. Data were recorded using a Multiclamp 700B amplifier and a Digidata 1440A interface controlled by Clampex 10.6 (Molecular Devices, USA). Signals were digitized at 10 kHz and low-pass filtered at 5 kHz. The recordings were performed on mCherry-expressing pyramidal neurons in dmPFC that were visualized under epifluorescence using a filter set (Olympus, Japan) with a monochrome CCD camera.

To measure the effect of CNO administration on hM3DGq and hM4DGi in dmPFC labeled neurons, brain slices containing the dmPFC were chosen for recording. To test hM3DGq positive neurons, CNO (10 μM) was applied to bath solution after 5 min recording under current-clamp mode. To test hM4DGi positive neurons, voltage responses to a current pulse (600 ms, 100 pA) were recorded before and 10 min after CNO (10 μM) application to the bath solution.

For analysis of membrane properties, the membrane potential was held at −70 mV under current-clamp mode. Depolarizing current steps (600 ms in duration, 50 pA increments) were used to detect action potential (AP). AP threshold was determined by differentiating the AP waveform and setting a rising rate of 20 mV ms^{-1} as the AP inflection point. AP amplitude was measured from the equipotential point of the threshold to the spike peak. AP duration was measured at the half-width of the spike. Data were excluded when the resting membrane potential of neurons was above −55 mV and AP did not have overshoot.

CFA-induced inflammatory pain

Mice were anesthetized with isoflurane. The plantar surface of the left hindpaw was cleaned by 75% ethanol, before a total of 50 μL CFA was injected intraplantarly. For controls, equal volume of normal saline was injected.

Behavioral tests

Thermal and mechanical pain thresholds

Each mouse was handled for 5 min and adapted in a plexiglas cube (7.5 cm × 4.5 cm × 4.5 cm) for 30 min per day for 3 consecutive days before the first measurement. Thermal or mechanical pain thresholds were measured while the mouse stayed calm and awake.

Paw withdrawal latencies (PWLs) to thermal stimulus were measured by a focused radiant heat (20W of power) applied to either hind paw of the mice (Hargreaves Method, IITC Life Science, USA). PWLs were recorded five times and averaged as the thermal pain threshold. A cutoff value of 20 s was set to avoid possible tissue injuries.

Fifty percent paw withdrawal thresholds (50% PWT) in response to 0.02–1.4 g *von Frey* hairs (Stoelting, USA) were measured using the up-and-down method.[76] Each test began with a 0.16 g hair force delivered perpendicularly to the central plantar surface of either hind paw for 3 s. Positive responses included sudden paw withdrawal, flinching, or paw licking were recorded. 50% PWT of either hind paw was calculated using the following formula: $50\%\ PWT\ (g) = 10^{Xf+k\delta}/10{,}000$, where Xf is the handle-marking value of the final *von Frey* hair used, k is the tabular value for positive/negative responses pattern, and δ is the average interval (in log units) between *von Frey* hairs used.

Spontaneous nociceptive behaviors

Spontaneous nociceptive behavior was measured before thermal and mechanical pain thresholds test every time. Mice were placed in a transparent plastic chamber (7 cm × 4 cm × 4 cm) and videotaped for 20 min. Spontaneous nociceptive behavior was analyzed by counting the time duration of lifting and licking, or the bouts of flinching behaviors. Researchers were blind from animal grouping.

Open-field (OF)

Each mouse was placed in a box exposed (60 cm × 60 cm × 65 cm) to 60 lux illumination, with its activities videotaped for 5 min. Time spent (C.Time), distance traveled (C.Dis) in the central area (30 × 30 cm) and total distance traveled (T.Dis) in the field were measured using the SMART Video tracking software. The box was cleaned by 75% ethanol between tests.

Elevated plus-maze (EPM)

The elevated plus-maze test was performed on the next day of the open-field test, unless otherwise noted. Maze consisted of two open arms and two closed arms (5 × 30 cm and 15 cm wall height for the closed arms) was placed 50 cm above the floor in a 60 lux illuminated room. Each mouse was placed onto the center area, heading toward the same open arm, and videotaped in the following 5 min. Time spent (O.Time), numbers of entries (O.Entries) into open arms and total arm entries (T.Entries) were analyzed using the SMART software. Maze was cleaned by 75% ethanol between tests.

Conditioned place preference (CPP)

Mice were tested in a conditioning apparatus consisted of 2 equal rectangular compartments (15 cm × 15 cm × 25 cm) with distinct visual and tactile features. The apparatus was cleaned with 75% ethanol after each test.

During pretest session, mice were allowed to freely explore the whole box for 10 min. Time spent in either chamber was recorded. Mice were excluded if they spent more than 75% of the time in either compartment.

For hM3DGq-induced chronic pain-like test (Figure 6): During the conditioning session for 2 days, mice underwent ''pairing'' where they were individually restricted to one chamber for 30 min, after receiving CNO (1mg kg^{-1}, *i.p.*) injection in the morning. Six hours after first CNO injection, they were restricted to the other chamber for 30 min after receiving CNO (1mg kg^{-1}) and morphine (1mg kg^{-1}, *i.p.*, 2.5 mg mL^{-1} dissolved in sterile saline, First Pharmaceutical Factory of Qinghai, China) injection.[23] Chamber pairing was counterbalanced in different mice.

For hM4DGi suppressed CFA model (Figure 7): During the conditioning session for 4 days, mice underwent ''pairing'' where they were individually restricted to one chamber for 30 min, after receiving vehicle injection in the morning. Four hours after the first injection, they were restricted to the other end chamber for 30 min after receiving CNO (1mg kg^{-1}, *i.p.*) injection. Chamber pairing was counterbalanced in different mice.

On the following test day, mice were allowed to freely explore the whole box for 10 min. Video was analyzed by SMART software. CPP score was calculated as $(T_{test} - T_{pretest})/T_{pretest} \times 100\%$. T_{test} was the time in the drug-paired (morphine chamber for hM3DGq group and CNO chamber for hM4DGi gruop) chamber on the test day. $T_{pretest}$ represented the time in the drug-paired chamber on the pretest day.

QUANTIFICATION AND STATISTICAL ANALYSIS

Data were expressed as mean ± SEM. Single variable comparisons were made with two-tail paired or unpaired Student's t test. Group comparisons were made using either one-way or two-way analysis of variance (ANOVA) followed by Bonferroni *post hoc* tests. Chi-square test were used to compare proportions. Wilcoxon rank sum tests were used to compare *in vivo* neural firing rates. Kruskal-Wallis test with Dunn's *post hoc* test was used in the comparisons of three or more groups with abnormal distribution. Spearman's correlations were used to analyze correlation between two variables. All statistics were calculated using GraphPad Prism, Origin or MATLAB. $p < 0.05$ was taken as statistically significant. Detailed statistical analysis was shown in Table S1.